Design, Construction and Control of a Quadrotor Helicopter Using a New Multirate Technique

Camilo Ossa-Gómez

A Thesis

in

The Department

of

Electrical and Computer Engineering

Presented in Partial Fulfillment of the Requirements

for the Degree of Master of Applied Science (Electrical and Computer Engineering) at

Concordia University

Montréal, Québec, Canada

June 2012

CONCORDIA UNIVERSITY

School of Graduate Studies

This is to certify that the thesis proposal prepared

By: **Camilo Ossa-Gómez**

Entitled: **Design, Construction and Control of a Quadrotor Helicopter Using a New Multirate Technique**

and submitted in partial fulfilment of the requirements for the degree of

   Master of Applied Science (Electrical and Computer Engineering)

complies with the regulations of this University and meets the accepted standards with respect to originality and quality.

Signed by the final examining committee:

———————————————————— Dr. L. A. Lopes, Chair

———————————————————— Dr. Dr. R. Dssouli, Examiner, External

———————————————————— Dr. A. Aghdam, Examiner

———————————————————— Dr. L. Rodrigues, Supervisor

Approved by ————————————————————————————

Dr. W. E. Lynch, Chair

Department of Electrical and Computer Engineering

——

Dr. Robin A. L. Drew

Dean, Faculty of Engineering and Computer Science

ABSTRACT

Design, Construction and Control of a Quadrotor Helicopter Using a New Multirate
Technique

Camilo Ossa-Gómez

This thesis describes the design, development, analysis and control of an autonomous Quadrotor Uninhabited Aerial Vehicle (UAV) that is controlled using a novel approach for multirate sampled-data systems. This technique uses three feedback loops: one loop for attitude, another for velocity and a third loop for position, yielding a piece-wise affine system. Appropriate control actions are also computed at different rates. It is shown that this technique improve the system's stability under sampling rates that are significantly lower than the ones required with more classical approaches. The control strategy, that uses sensor data that is sampled at different rates in different nodes of a network, is also applied to a ground wheeled vehicle. Simulations and experiments show very smooth tracking of set-points and trajectories at a very low sampling frequency, which is the main advantage of the new technique.

"If we knew what it was we were doing,

it would not be called research, would it?"

— Albert Einstein

"There are trivial truths and there are great truths.

The opposite of a trivial truth is plainly false.

The opposite of a great truth is also true."

— Niels Bohr

ACKNOWLEDGEMENTS

TABLE OF CONTENTS

LIST OF FIGURES

LIST OF TABLES

Chapter 1

Introduction

1.1 Motivation

Uninhabited Vehicles (UVs) have motivated a significant amount of research in diverse fields during the last decades. UVs are no longer a topic of interest only for scientists and engineers, but also for the general public. From self-driving cars to autonomous home cleaning devices and radio-controlled mini air vehicles, UVs are getting closer to everyday life. Moreover, Uninhabited Air Vehicles (UAV), have attracted great attention, partly because of the many potential applications they have, such as mapping, surveillance, fire fighting, exploration, and support of rescue operations, to name a few. In particular, quadrotor helicopters are getting special attention during the last two decades. In addition to the obvious advantages of using UAVs in missions where hazardous conditions for human pilots are involved, a quadrotor offers some edges over fixed-wing aircrafts such as the ability of Vertical Take-off and Landing (VTOL) and hovering. Furthermore, its maneuverability and small size makes it suitable for indoor flight.

One of the main challenges of controlling a quadrotor comes from the fact that they are inherently unstable and some of their physical variables have a relatively fast dynamic

behavior. These characteristics require a fast sampling rate to maintain the system's stability. If there are wireless communications involved in the control tasks, the used protocol must be able to provide a transfer rate fast enough that will not add significant delays that could negatively affect the performance of the aircraft.

Fly-by-wireless (FBW) is a technology trend driven mainly by the aerospace industry, aiming at improving the efficiency and reliability of aircrafts while reducing operational costs from maintenance by decreasing the amount and complexity of its wiring. An evolution of fly-by-wire technology, FBW not only keeps the assets of its predecessor, but also adds advantages such as scalability, flexibility, less wiring weight and reduced chances of hardware failure at connectors and wires, amongst others [1].

Multirate control, on the other hand, is an intuitively efficient way to control systems in which several variables with different dynamical time-constants are interacting with each other. It is a known fact that fast variables require faster sampling rates than the slower ones. In addition, when several sensors are used in a system they usually have different update rates. In modern control applications, including vehicles, most sensors are digitally interfaced with the control processing unit at given sampling rate. That rate depends on a number of factors that are specific to each sensor; they usually have embedded processing units dedicated to perform specific tasks that are needed to obtain reliable measurements of the variables. Reading the analog measurements of the sensors, filtering the signals and managing the communication with the main processor are some of the typical tasks of these embedded processors. Therefore, each sensor has a different sampling frequency. Multirate control takes advantage of this fact, allowing different rates for different sets of variables in the control loop.

A controller that is able to handle multiple rates has two main advantages:

1. It can manage a system in which different sensors provide measurements at different fixed rates

2. It allows to optimize the sampling frequencies and computational load for the case

2

of sensors that can be polled.

A controller that is able to handle multiple rates has two main advantages: First, it can manage a system in which different sensors provide measurements at different fixed rates; second, it allows to optimize the sampling frequencies and computational load for when sensors that can be polled are used.

In some applications where a Global Positioning System is not available, such as the Mars Exploration Rovers, position estimations are based on Visual Target Tracking (VTT) and Visual Odometry (Visodom). The position updates using these systems can take up to 1 minute using VTT, and 2-3 minutes using Visodom [2]. When such low sampling frequencies are the only source of information for position in a navigation system, multirate control techniques that are robust under these conditions are required.

When considered separately, the topics mentioned in the previous paragraphs have been active research fields during the last decades. However, to the best of our knowledge there are no results combining these three topics in the open literature. The goal of this thesis is threefold. The first component is the development of a quadrotor helicopter to be used as a test platform to implement the control strategies and algorithms. The second is to design controllers using FBW technology in the test platform. The network limitations and constraints will be analyzed to predict how they influence the system's stability and performance, and the output of that process will be considered during the control design to develop algorithms that are compliant with these possible limitations. Finally, a multirate controller will be designed, analyzed and implemented, inspired by the nature of the different dynamical behavior of the variables involved during the operation of the quadrotor. Additionally, it will be shown that the developed multirate strategy is suitable for a wide variety of vehicles, and this strategy will also be implemented on an autonomous land rover.

1.2 Literature Survey

1.2.1 Quadrotor helicopters

The first quadrotor helicopter took off in 1922. It was built by George de Bothezat for the United States Army Air Service, and although the prototype was successful, the program was canceled one year later, allegedly because of its mechanical complexity, reliability problems, and because it was unresponsive and underpowered [See Figure 1.1]. Although other projects further explored four-propeller helicopters, there is few information in the open literature [3].
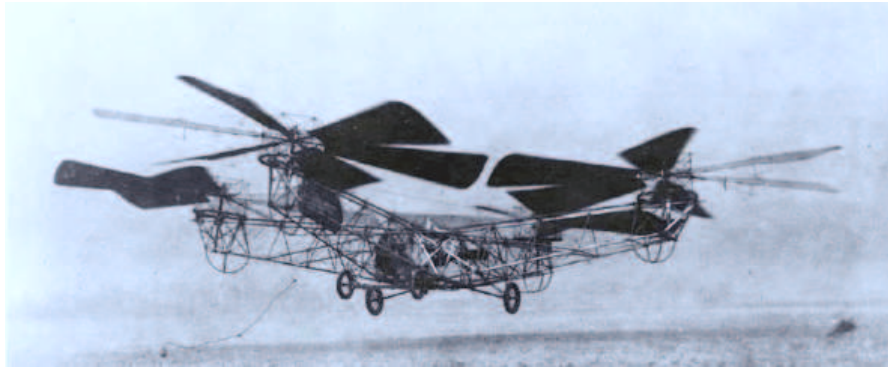
Figure 1.1: De Bothezat quadrotor, 1922 [4]

The four-propeller architecture started to gain relevance during the 1990s and became an active research field since the beginning of the last decade. Projects such as the HoverBot [5], and the Mesicopter [6] explored the possibility of an electrically powered quadrotor. Atug et. al. [7] were the first ones to use the term quadrotor in a publication in the open academic literature. They modeled the quadrotor using Newton-Euler's laws and attempted its stabilization and tracking using visual feedback as the main sensor. Later, Moktari et. al. [8] designed a state parameter control based on Euler angles and state position observer for a nonlinear dynamic model. Several different strategies such as sliding mode observers [9], neural networks [10] and PD^2 feedback based on the compensation of the Coriolis and gyroscopic torques [11], to name a few, were also implemented during

4

the last decade.

More recent research on quadrotor control has also addressed several approaches, including model predictive control [12], dynamic inversion [13], nested saturations, back-stepping and sliding modes [14] and H_∞ control [15]. Multirate control has been addressed in [16] using lifting operators, where only attitude and altitude were considered, reducing the problem to a fully-actuated system.

Figure 1.2: Commercial modern Quadrotor UAVs from ETH Zurich [17]

Mellinger et. al. [18] from the GRASP Laboratory at University of Pennsylvania and Hoffmann, et. al. [19] from Stanford and Waterloo Universities, have focused on trajectory generation and control for aggressive maneuvers with quadrotors. D'Andrea et. al. have conducted research in a number of different fields and applications for quadrotors such as ball juggling [20], trajectory generation [21], acrobatic maneuvers [22], choreography with several helicopters [23] and control of an inverted pendulum mounted on a quadrotor [24]. Figure 1.2 shows a commercial modern quadrotor used in research at the GRASP Laboratory.

1.2.2 Fly by wireless

The first time that the term "Fly-by-wireless" was used in the open academic literature was in 2001 in a paper by P. Wiberg and U. Bilstrup [25]. They discussed the possibility

of implementing a FBW channel in an aircraft and discussed the order of magnitude of the bit error probability. Carvalhal et. al. [26], [27] were the first ones to implement FBW technology in a UAV fixed-wing aircraft using Bluetooth protocol. Belapurkar et. al. [28] and H. Liu [29] proposed Wireless Sensor Networks (WSN) for aircraft control, health management systems and fault diagnosis. Figure 1.3 illustrates a FBW aircraft control system scheme implemented on a military aircraft [28]. Taajwar et. al. [30] propose the use of a CDMA and single-wire-line technology as a potential solution for Fly-by-wireless/less-wire. Elgezabal et. al. [32] did an extensive state of the art exploration of wireless data transmission to provide technological foundation for future intra-aircraft wireless applications. S. Chilakala [33] and D. Hope [34] implemented IEEE 802.11 and ZigBee protocols in a UAV. The former also studies intra-aircraft wireless propagation phenomena such as resonant cavity, and reverberation chamber.
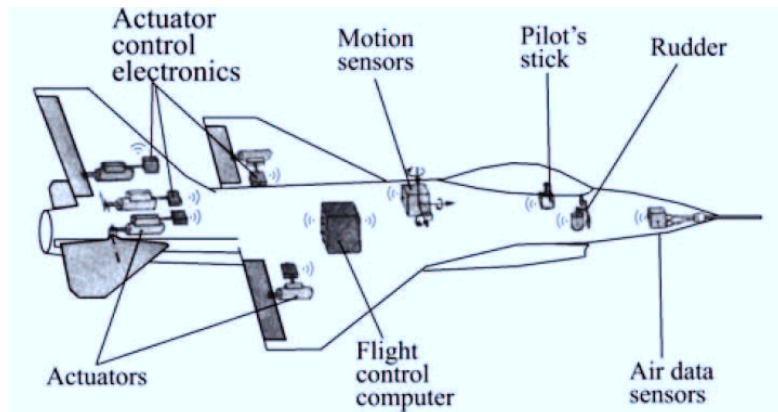
Figure 1.3: Fly-by-wireless aircraft flight control system [28]

1.2.3 Multirate control

Research on multirate control started in the 1950's. D. Kranc [35], started the analysis of sampled-data systems with different sampling rates using Z-transform methods. B Friedland [36] developed the concept of lifting operators, setting the general framework for multirate control systems analysis. J. Johnson et. al. [37] further continued the analysis of

6

multirate digital control systems by studying the error induced by the quantization of signals. D. Flowers et. al. [38] proposed a method to simplify the characteristic equations of multirate control systems and proposed the first design techniques specifically conceived for this class of systems. Boykin et. al. [40] proposed the analysis of multirate control systems using vector operators to obtain modified Z-transforms.

Recent results on multirate control systems include techniques to eliminate ripple [41], applications to networked Internet-based control systems [43] and tracking control based on multirate feedforward control with generalizations of sampling periods [42]. Recent applications include visual servoing of manipulators [44] and radial control tracking in high-speed DVD players [45].

1.3   Objectives and contributions

The main objectives and contributions of this thesis are twofold. In terms of theory, the main novelty is the proposed multirate control technique with a proof of stability for the case of kinematics control. Although multirate control is not new, the proposed technique follows a new approach that splits tightly coupled state variables in nested loops that are inspired by the nature of the studied vehicle's models and typical sensors. In terms of the application, the fly-by-wireless approach applied to a quadrotor helicopter is the main novelty.

The main objectives of this thesis are:

- Design and build a quadrotor helicopter controlled using fly-by-wireless technology.

- Propose a multirate control strategy that is applicable to quadrotor helicopters in particular, and underactuated vehicles in general.

The main contributions of this thesis are the following:

- Developing an Uninhabited Air Vehicle that is controlled from a Ground Control Station (GCS) using fly-by-wireless technology, providing a modular setup for research in both networked control and UAV autonomous control.

- Proposing a new control strategy for a class of underactuated vehicles using a multirate approach.

- Applying the proposed strategy to an experimental setup including a quadrotor helicopter and a land vehicle.

1.4   Structure of the Thesis

The rest of this thesis is structured as follows. In Chapter 2, the design, construction and modeling of the quadrotor helicopter is detailed. First, the requirements, specifications and design considerations are stated and explained. Then, the mechanical and electrical design and construction process is summarized and illustrated. Finally, the system is modeled as a nonlinear dynamical system, and the parameters are characterized. Subsequently, in Chapter 3, two case studies are introduced: a longitudinal model of the quadrotor and a land rover. For these two examples, the kinematics control is addressed using the proposed multirate technique. Simulation results are presented, as well as the stability and velocity of convergence analysis. Next, in Chapter 4, the dynamics control is discussed. Considering the rotational dyanamics, the system is analyzed and an piecewise-affine expression for the closed-loop is found. Experimental results are also presented for both case studies. Conclusions are drawn in Chapter 5.

This thesis is based mainly on the following two papers:

- Camilo Ossa-Gómez, Miad Moarref and Luis Rodrigues, "Design, Construction and Fly-By-Wireless Control of an Autonomous Quadrotor Helicopter", *4th IEEE / CANEUS Fly-by-wireless Workshop*, Montreal, QC, Canada, 2011.

8

- Camilo Ossa-Gómez and Luis Rodrigues, "Multi-Rate Sampled-Data Control of a Fly-by-wireless Autonomous Quadrotor Helicopter", *Proceedings of the 25th IEEE Canadian Conference on Electrical and Computer Engineering CCECE'2012*, Montreal, QC, Canada, 2012.

Chapter 2

Quadrotor Design, Construction and Modeling

The first part of this chapter describes the process of conception, design and construction of the quadrotor helicopter used for the work presented in this thesis. This UAV is developed at the HYbrid CONtro Systems Laboratory of Concordia University. In the second part, the process of modeling the quadrotor is presented.

2.1 General requirements, specifications and design considerations

The HYCONS quadrotor helicopter was conceived as a research platform for networked control. Therefore, one of the main requirements was to set up a wireless network to send sensors and control signals between the UAV and the GCS. Fly-by-wireless and sampled-data multirate networked control have been the main two fields in which research has been conducted using this platform, developed at the HYCONS Laboratory of Concordia University.

The quadrotor was designed for indoor flight in a standard-height ($\sim 3m$) laboratory.

A cube-shaped safety cage with a 2.5m side was built; therefore the size should be designed accordingly. Flying systems are made of light materials in order to reduce the required lift to counteract its weight. Besides the main obvious design requirements such as the weight/throttle ratio and stiffness, an extra effort was made to add certain features such as a high modularity and flexibility. The two latter characteristics are key in the development of a vehicle that is going to be used in several different kinds of tests that might involve the need of adding and subtracting significant hardware parts such as sensors and on-board processing units, among others.

2.2 Wireless communications

The first goal of the quadrotor was to analyze the behavior of such a UAV when being controlled over a fly-by-wireless network. The proposed approach consists of performing all control computations off-board—on the GCS—using the measurements made by the on-board sensors and send the control inputs back to the quadrotor to command the motors. Figure 2.1 illustrates this networked control approach. The first step was to find an appropriate wireless communication standard based on previous research in FBW. S. Chilakala [33] conducted a survey on suitable wireless protocols that might be used for FBW applications. Comparisons and tests were made considering data rate, range and power consumption for several IEEE 802 protocols. According to the conclusions of the previously mentioned work, the ZigBee standard (IEEE 802.15.4) features a good compromise of low power consumption and one of the longest distance ranges. XBee is a Commercial-Off-The-Shelf (COTS) hardware that uses the ZigBee standard with the additional advantages of a low weight and small size [46]. In addition to this, the experience of several users and researchers who discuss their experiments and tests in community based websites [47], [48], show that XBee is a reliable and suitable protocol for UAV applications.
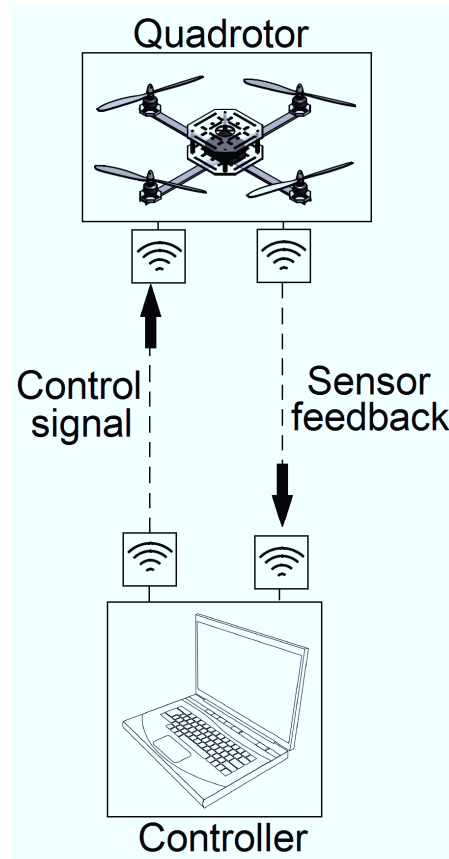
Figure 2.1: Proposed wireless control approach for the quadrotor

Based on the previous statements, XBee is chosen as the solution for this project's wireless communications. Furthermore, it allows to connect any device with a serial port to the wireless network, either a PC, a Micro Controller Unit (MCU), or any other electrical device with such capabilities. The selected XBee modules operate within the Industrial, Scientific and Medical (ISM) radio band at a frequency of 2.4GHz. Figure 2.2 shows a picture of two of the XBee modules produced by the company Digi International Inc.

2.3 Electronics and sensors

The electronics implemented in the platform can be divided into two main blocks—the on-board electronics and the GCS. Figure 2.3 shows a schematic picture of the electronics involved in the control of the quadrotor. The two main groups are identified as separate
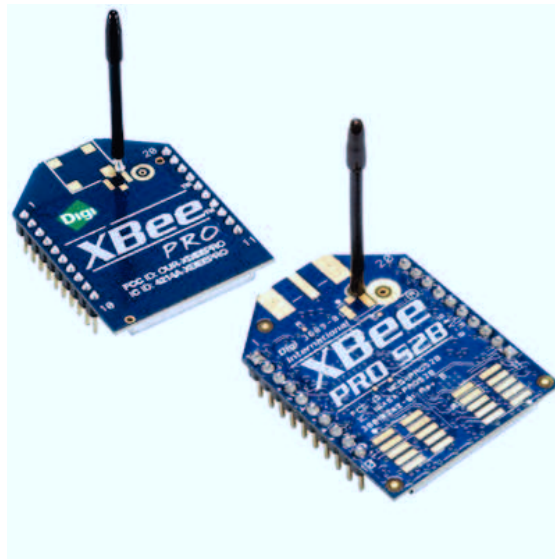
Figure 2.2: XBee Modules [46]

blocks connected through an IEEE 802.15.4 wireless network that is implemented using XBee modules. A detailed description of each functional block is given in the following subsections.

2.3.1   Processing Unit

The HYCONS quadrotor was conceived as a research platform for wireless networked control with an off-board controller, as it was mentioned at the beginning of this chapter. The required processing capability on board was not a key factor for selecting a processor unit. Instead, other factors such as small size, light weight, ease of update and availability of programming libraries to speed up the development process played a major role. The input/output requirements of the on-board processing unit are as follows:

- Three Serial ports

- One SPI port

- Four Pulse-Width Modulation (PWM) outputs

- Four analog inputs

13
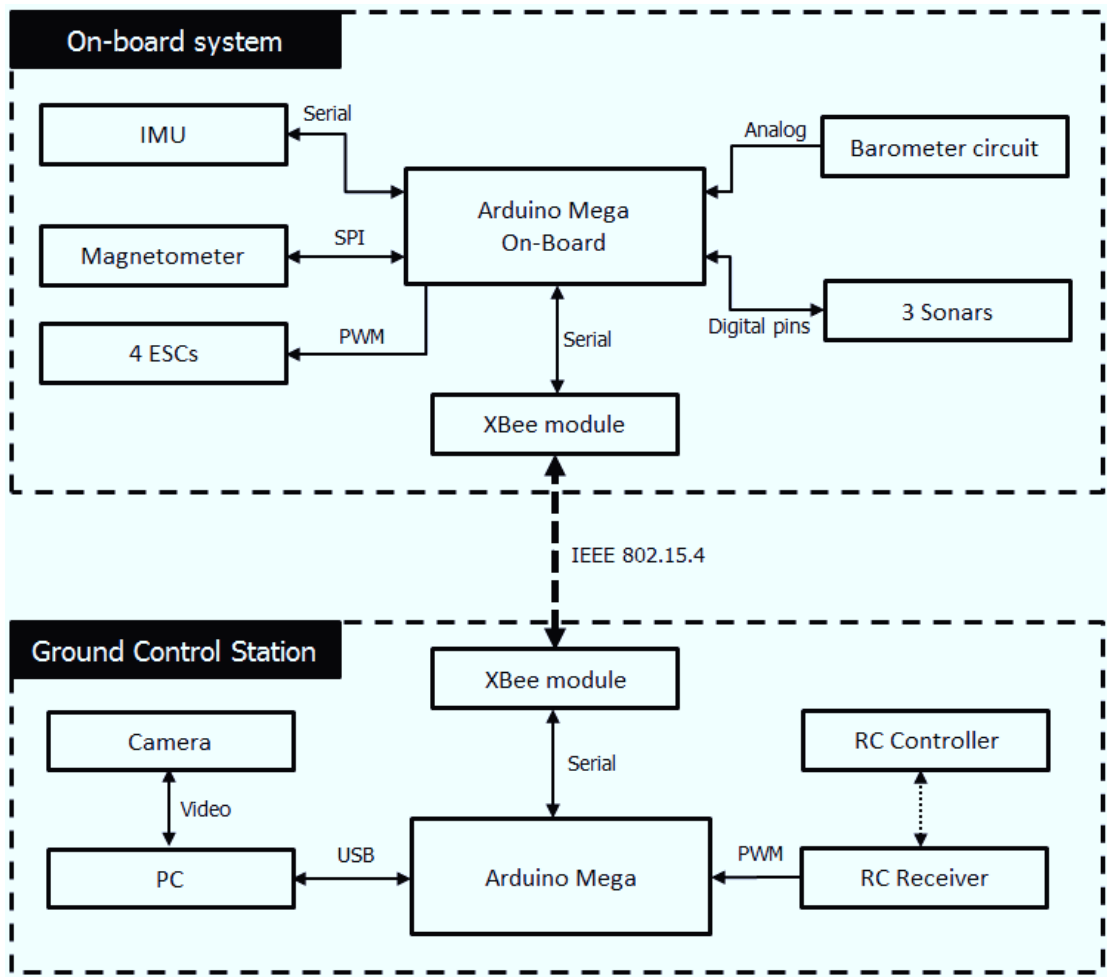
Figure 2.3: Electronics schematic

- Built-in voltage regulation

- At least twelve input/output digital pins

Based on the requirements, the Arduino Mega Board was chosen as on-board processing unit. It is a powerful open-source low cost board that meets all required specifications, with some additional advantages. Amongst its advantages, it features a cross-platform development environment on C++ with extensive libraries that help speed up the development process. There is also a significant amount of online resources and examples that are very useful in the learning process.

14

In addition to this, the Arduino Mega has plenty of digital input/output and analog pins that are useful for tests and leaves room for further development, such as adding new sensors, actuators and interfaces. Figure 2.4 shows a picture of the Arduino Mega Board.
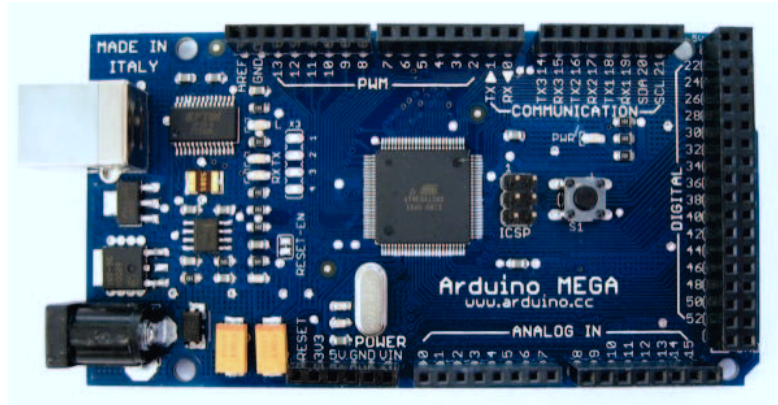
Figure 2.4: Arduino Mega Board [49]

2.3.2 Inertial Measurement Unit (IMU)

The main sensor used in the HYCONS quadrotor is a MicroStrain 3DM-GX1 Inertial Measurement Unit. It integrates three accelerometers, three gyroscopes and three magnetometers with an embedded microcontroller to provide a measure of the Euler angles, its rate of change and the accelerations of the UAV at a rate of 76Hz. Figure 2.5 shows a picture of the 3DM-GX1 IMU. It has an integrated Kalman Filter to fuse the sensor's information and provide a clean stream of data. In addition to the mentioned specifications, the selected IMU has the advantages of a small size and light weight, making it suitable for this application. Its interface is a standard RS232 communication. Since the Arduino Mega does not support the standard voltages of a RS232 communication of $\pm 12V$, a signal adapter was used. The selected adapter is a Sparkfun RS232 Shifter. It transforms the voltages from the RS232 to TTL levels, so the Arduino can interpret the signals.

Figure 2.5: MicroStrain 3DM-GX1 IMU [50]

2.3.3 Electronic Speed Controllers (ESC)

Four ESCs are used to control the electric motors. They take a PWM signal as input and generate the control signals for the three phases of the outrunner brushless DC motors. Based on the motors' requirements, they must be able to handle a continuous current of 12A and a maximum burst current of 15A. The selected ESCs are the Thunderbird-18 ESCs. They are small, light and can deliver up to 18A [51]. They also provide a 5V regulated output that is used to power the TTL logics.

2.3.4 Magnetometer

An extra magnetometer was added to improve the stability of the yaw measurement, since it was presenting a slow drift, which is one of the characteristics of inertial measurement systems. The Sparkfun Triple Axis Magnetometer Breakout - HMC5883L was selected for its low current draw, small size and light weight. This device is connected to the Processing unit through an SPI port. A command is given to the magnetometer every time

a new measurement is needed, and it returns a stream of data containing the requested information.

2.3.5 Ultrasonic range finder

In order to measure the distance to the ground and surrounding walls, three sonar sensors were added. One is pointing downwards to measure the distance to the floor. The other two are pointing towards the quadrotor's X and Y axis, which are orthogonal directions in the horizontal plane during hovering. The MaxBotix LV-MaxSonar-EZ4 was the selected sensor. Each sonar is connected to the processing unit using two digital pins, one to command a new range measure, and a second to detect the output signal. The range is determined by measuring the time it takes for the ultrasonic signal that is sent by the sensor to be reflected towards the sensor by a surface. The delay of the output signal is proportional to the distance to the nearest object in front of the sensor. Figure 2.6 shows a picture of the selected Ultrasonic range finders.

Figure 2.6: Maxbotix LV-MaxSonar-EZ4 [52]

2.3.6 Machine Vision System

A machine vision system was implemented to determine the position of the quadrotor with respect to the workspace. A marker is placed on the vehicle and a camera is mounted on top of the workspace pointing downwards. The camera captures images that are processed

by a computer running Matlab/Simulink in real-time using the RTsync Blockset [53]. A custom S-function block that is running code written in C++ using the OpenCV library [54] processes the stream of images to identify the marker and output its position and orientation. Figure 2.7 shows a picture of the camera used for this purpose.

Figure 2.7: Machine Vision system camera

HYCONS Quadrotor		
Component	**Reference**	**Details**
Motors	E-flite 370	Brushless outrunner
Propellers	APC 10 x 4.7	Composite polymer
ESCs	Thinderbird 18	18A maximum current
IMU	MicroStrain 3DM-GX1	76 Hz frequency
Processing unit	Arduino Mega	16MHz clock
Wireless device	XBee modules	Frequency 2.4GHz
Magnetometer	HMC5883L	3-axis, 5 milli-gauss res.
Sonars	LV-MaxSonar-EZ4	20Hz reading rate
Barometric sensor	MPX4115A	Sensitivity: 46 mV/kPa

Table 2.1: HYCONS Quadrotor main components

2.4 Mechanics

2.4.1 Mechanical structure

The mechanical structure of the HYCONS quadrotor was designed as a modular platform that can be easily reconfigured to add sensors, processing units, communication and other devices. Figure 2.8 shows a render made in the Computer Aided Design (CAD) software package used in the design of the vehicle and Figure 2.9 shows the vehicle that was built based on this design.
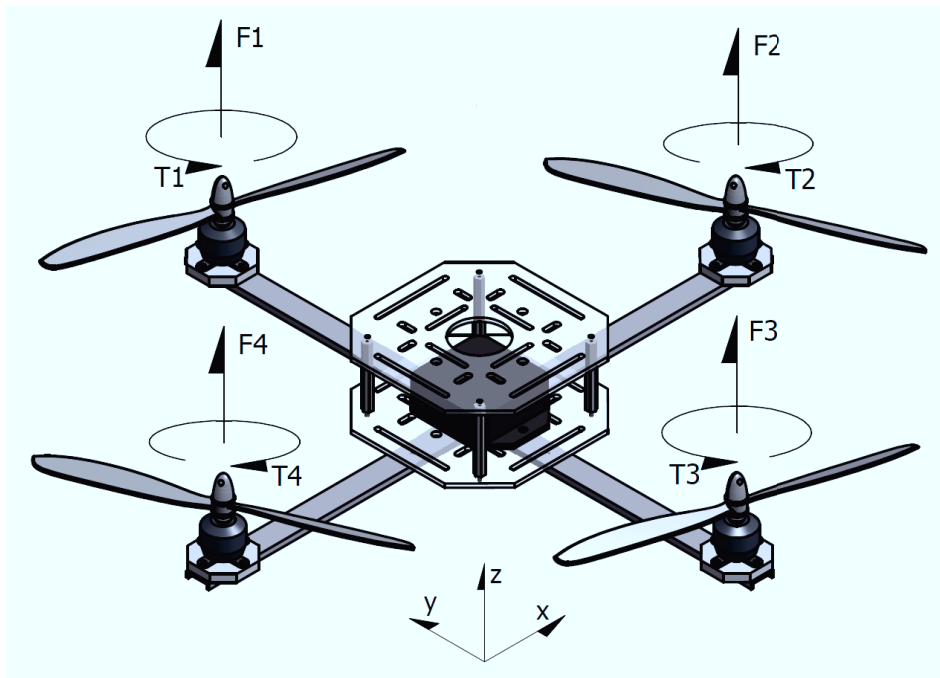
Figure 2.8: Render from the CAD model of the quadrotor.

Besides the main obvious design requirements such as the weight/throttle ratio and stiffness, an extra effort was made to add certain features such as a high modularity and flexibility. The two latter characteristics are key in the development of a vehicle that is going to be used in several different kinds of tests that might involve the need of adding and subtracting significant hardware parts such as sensors and on-board processing units, among others.

Two main materials were used: Polyoxymethylene (POM) and a general purpose aluminum alloy: 6063. The key characteristic of both materials is a high stress resistance to weight ratio. The Polyoxymethylene is an engineering thermoplastic that can be formed using a number of different manufacturing techniques. In addition to its high stress resistance to weight ratio, it has the additional advantage of a good machinability. The custom design of the plates and some connectors were made from sheets of POM using a CNC laser cutter. The aluminum alloy used for the arms of the quadrotor is a non-ferrous metal widely used in aerospace applications. The parts were made from standard square tubes that were cut using a CNC mill and drill. The fasteners are 4-40 stainless steel socket head cap screws, washers and nuts.

Figure 2.9: Picture of the HYCONS quadrotor

2.4.2 Motors and propellers

The selected motors are the E-flite 370 Brushless Outrunners. These motors are recommended for propellers in the range of 8x3.8 to 10x4.7. They work at a voltage range of 7.2-12V; therefore, a 2-cell or 3-cell LiPo battery can be used. Table 2.2 summarizes the most relevant characteristics of these motors. The selected propellers are composite APC

10x4.7, which are the largest recommended propellers for the E-flite 370 motors. Two of them are designed to rotate in the "regular" sense, which is counter-clockwise, and the other two are "pusher" propellers, and are designed to rotate clockwise. The final setup is summarized in Table 2.1.

E-flite 370	
Type	Brushless outrunner
Voltage	7.212
RPM/Volt (Kv)	1360Kv
Resistance (Ri)	.10 ohms
Idle Current (Io)	1.00A @ 10V
Shaft Diameter	3.17mm (1/8 in)
Overall Length	25mm (1.00 in)
Weight	45 g (1.6 oz)
Overall Diameter	28mm (1.10 in)
Diameter	28 mm (1.1 in)
Length	25 mm (1 in)
Continuous Current	12A
Maximum Burst Current	15A (15 sec)
Cells	610 Ni-Cd/Ni-MH or 23S Li-Po

Table 2.2: E-flite 370 Brushless Outrunner Motor characteristics. Information extracted from [55]

2.5 Modeling

Quadrotor helicopters have six degrees of freedom with respect to an inertial reference frame. They can have displacements along the coordinate axes (X, Y, Z) and three rotation angles about the quadrotor's axis, described by Euler angles, ϕ (roll), θ (pitch), and ψ (yaw). Quadrotors are controlled by changing the thrust produced by each propeller. This is achieved by giving appropriate speed commands Ω_i^c to each motor, defined as:

$$
\begin{cases}
\Omega_1^c = u_1 - u_2 + u_4 \\[2mm]
\Omega_2^c = u_1 - u_3 - u_4 \\[2mm]
\Omega_3^c = u_1 + u_2 + u_4 \\[2mm]
\Omega_4^c = u_1 + u_3 - u_4
\end{cases}
\tag{2.1}
$$

where u_1, u_2, u_3 and u_4 are the outputs of the altitude, roll, pitch and yaw controllers, respectively.

In [56], the system (2.2) is used to describe the dynamics of the quadrotor, based on the following two assumptions:

- The quadrotor rotates around its center of mass, where the origin of the body-fixed frame in located.

- The axis of the body-fixed frame coincide with the body principal axes of inertia, causing $I_{xy} = I_{yz} = I_{xz} = 0$.

The system model is

$$
\begin{cases}
\dot{X} = u \\[2mm]
\dot{u} = (s_\psi s_\phi + c_\psi s_\theta c_\phi) u_1 / M \\[2mm]
\dot{Y} = v \\[2mm]
\dot{v} = (-c_\psi s_\phi + s_\psi s_\theta c_\phi) u_1 / M \\[2mm]
\dot{Z} = w \\[2mm]
\dot{w} = -g + (c_\theta c_\phi) u_1 / M \\[2mm]
\dot{\phi} = p \\[2mm]
\dot{p} = \dfrac{I_{yy} - I_{zz}}{I_{xx}} \dot{\theta}\dot{\psi} - \dfrac{J_{TP}}{I_{xx}} \dot{\theta}\Omega + \dfrac{u_2}{I_{xx}} \\[3mm]
\dot{\theta} = q \\[2mm]
\dot{q} = \dfrac{I_{zz} - I_{xx}}{I_{yy}} \dot{\phi}\dot{\psi} + \dfrac{J_{TP}}{I_{yy}} \dot{\phi}\Omega + \dfrac{u_3}{I_{yy}} \\[3mm]
\dot{\psi} = r \\[2mm]
\dot{r} = \dfrac{I_{xx} - I_{yy}}{I_{zz}} \dot{\phi}\dot{\theta} + \dfrac{u_4}{I_{zz}}
\end{cases}
\tag{2.2}
$$

where:

- $s_{(\cdot)} = \sin(\cdot)$, $c_{(\cdot)} = \cos(\cdot)$

- M is the mass of the quadrotor

- g is the acceleration of gravity on the surface of earth

- I_{kk} is the body moment of inertia around the k axis

- J_{TP} is the rotational moment of inertia around the propeller axis

- $\Omega = -\Omega_1 + \Omega_2 - \Omega_3 + \Omega_4$, where Ω_i is the rotational speed of propeller i.

The state vector is defined as

$$x = \begin{bmatrix} \Gamma^T & \Theta^T \end{bmatrix}^T, \tag{2.3}$$

where

$$\Gamma = \begin{bmatrix} X & u & Y & v & Z & w \end{bmatrix}^T \tag{2.4}$$

and

$$\Theta = \begin{bmatrix} \phi & p & \theta & q & \psi & r \end{bmatrix}^T. \tag{2.5}$$

The inputs are arranged in the vector

$$u = \begin{bmatrix} u_1 & u_2 & u_3 & u_4 \end{bmatrix}^T. \tag{2.6}$$

The above model concludes this Chapter. The process of conception, design and construction was described in the first half; the second part showed the process of modeling the vehicle under certain conditions, stated in section 2.5. In the next two chapters, the kinematics and dynamics control of the two case studies is discussed.

Chapter 3

Kinematics control

In the following two chapters, two different case studies of UVs are used to describe the proposed approach to multirate control. This chapter focuses on one of the two main components of the system: the kinematics. In Chapter 4, the dynamics are discussed, the system is analyzed considering both dynamics and kinematics, and the experimental results are presented. The use of expressions Kinematics/Dynamics control refers to the nature of the variables that are considered in each approach. In kinematics control, only position, orientation and its derivatives are considered. In dynamics control, the causes of changes in position, orientation and its derivatives (i.e. torques and forces) are also considered.

The case studies addressed in this thesis are:

- a quadrotor helicopter, and

- a land rover.

In the first part of this Chapter, some general concepts and the notation is discussed. Later, the two case studies are presented. To conclude, the stability analysis and velocity of convergence of the proposed multirate control technique is presented.
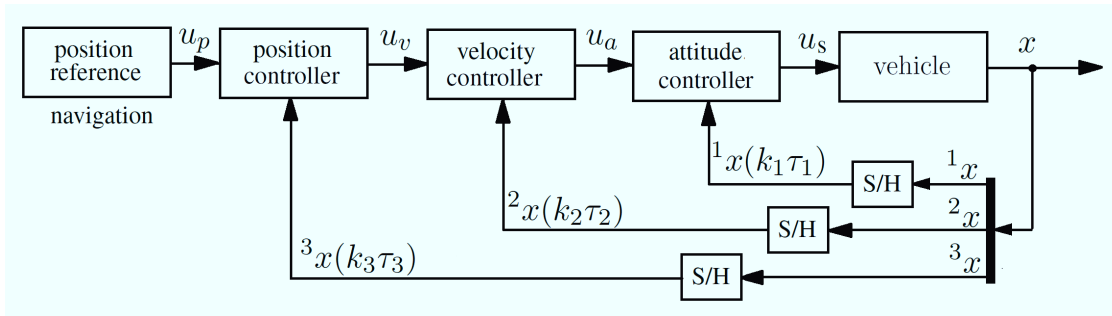
Figure 3.1: Multirate control loops

3.1 General concepts and notation

The approach described in this thesis, splits the control tasks into different loops to allow different sampling rates for each one. As mentioned in Chapter 1, this is practically relevant in several applications. An example of these applications is when multiple sensors are implemented in a system and each of them provide sampled information at a different rate. Another case in which multirate control is practically relevant is networked control. In the latter case, processing units and sensors are located in different nodes of a network, and the signals are affected by network-induced delays and sampling rates that are limited by the capability of the links.

The general idea is described in Figure 3.1. The proposed control algorithm splits the tasks in different loops, as follows. Three feedback loops, $m = 1, 2, 3$, are given. Each loop has a time-varying sampling period τ_m, whose upper bound $\overline{\tau_m}$ is known. The first loop, which is computed every τ_1 seconds, contains an attitude controller; this controller has an input reference u_a, and gives to the vehicle's actuators the control signal u_s that is required to achieve the commanded control task. The second loop controls the velocity with a sampling time of τ_2 seconds. It has a input reference u_v, and outputs the attitude reference u_a to the attitude controller. The third one, that controls the position, has an input reference u_p, which is a desired position, waypoint or path. It gives the velocity reference u_v to the second loop.

The state vector is split into three sub-states, $^m x$, according to their sampling frequencies, as shown in Figure 3.1. Due to its sampled nature, the sub-states measurements, are written as

$$^m x(k_m \tau_m), \text{ for } t \in [k_m \tau_m, (k_m + 1)\tau_m), \tag{3.1}$$

where $k_m \in \mathbb{N}$, and $k_m \tau_m$ and $(k_m + 1)\tau_m$ are two consecutive sampling times at which the state is measured.

The controls loops must be chosen appropriately, in such way that

$$\tau_3 \geq \tau_2 \geq \tau_1 \tag{3.2}$$

Evidently, if the sampling rates are equal, the closed-loop system becomes a regular sampled control system that has only one sampling frequency. The advantages of the proposed multirate control technique are more evident when the difference between at least two of the sampling periods is large. Roughly speaking, the proposed multirate control technique has two main steps:

Step 1: State space partitioning

The state vector is partitioned in sub-states. The states contained in each group must have the same sampling frequency and also represent the same kind of physical variable. For example, angles and angular rates must be grouped together. A reason for grouping certain variables together is the fact that typically, sensor packages such as inertial measurement units, provide information about several variables in the same data stream, therefore, the measurements are made at the same frequency. For each vehicle, the state variables are split in a different way, depending on specific characteristics of its model, as it will be shown in the case studies.

Step 2: Design the controller for each loop

The first block of loop m is a controller that takes as input the reference given by

the preceding loop controller $m+1$, updated every τ_{m+1} seconds. In turn, it computes the control input that is given to the next block at a rate of τ_m^{-1} Hertz. The first block in the system takes the position, waypoint or path reference defined by the control objective. The last block gives the physical inputs to the plant's actuators.

The mth loop controller is designed in such a way that the states that are controlled in the loop ($^m x$), track the reference given to the loop before the next reference comes (τ_{m+1} seconds after). The faster the tracking is, compared to τ_{m+1}, the better the achieved performance is. The inner controllers are designed first, in such a way that each step is validated with the plant model before proceeding to the next loop.

We start by analyzing the quadrotor helicopter.

3.2   Quadrotor Helicopter

The kinematic control of the HYCONS quadrotor is discussed in this section. To illustrate better the proposed control approach, the motion along one of the quadrotor's axis is isolated. Quadrotor helicopters can move in the X and Y axis thanks to the accelerations that are produced when the vehicle tilts. Due to the inclination angle, the thrust generated by the propellers has an horizontal component. If the quadrotor pitches with zero yaw, an acceleration is produced along the X axis; in an analog way, when it rolls, an acceleration is produced along its Y axis.

The dynamics of motion along the X and Y axes of the body-fixed frame are identical. Assuming that ϕ and ψ are stabilized to zero, and only displacements along the X axis and rotations about the Y axis, are considered, equation (2.2) is reduced to equation (3.3). To facilitate the illustration, the analysis is made in one of the two horizontal axes, only considering displacements along the X axis and the pitch angle. It yields a longitudinal motion model. Figure 3.2 shows an illustration of the longitudinal model used in this section.
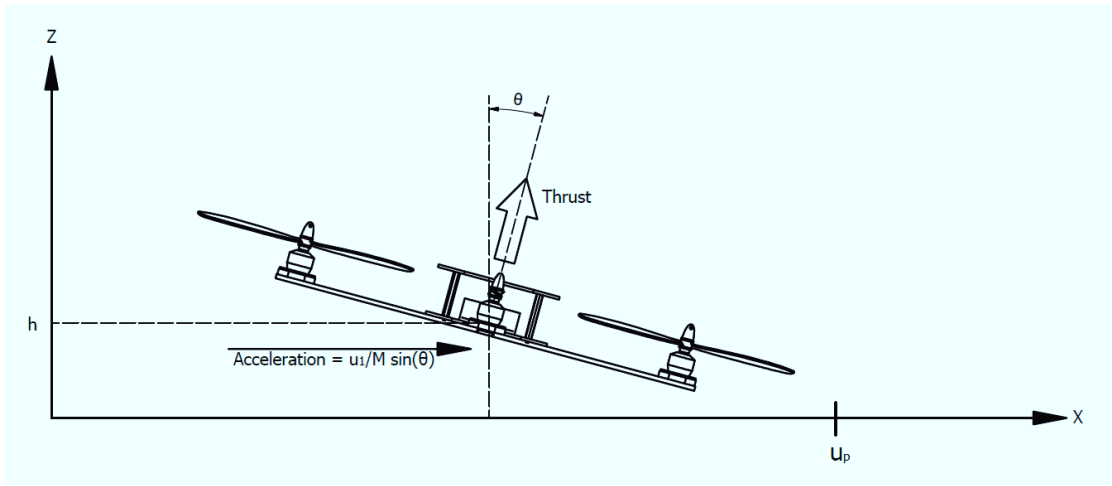
Figure 3.2: Longitudinal model of the quadrotor.

$$\begin{cases} \dot{X} = u \\ \dot{u} = u_1/M \sin \theta \\ \dot{\theta} = p \\ \dot{p} = u_3/Iyy \end{cases} \tag{3.3}$$

Note that the dynamic equations for Y, Z, ϕ and ψ, and their rates of change, v, w, q and r are no longer considered in this reduced model. However, since the dynamics of the two horizontal axes is identical, the same controller can be applied to control the motion along the Y axis and the roll angle (ϕ). The variable u_1 is the altitude controller input, which has units of force $[g\,m\,s^{-2}]$. The pitch controller input, u_3, which has torque units $[g\,m^2\,s^{-2}]$ is the input to control model (3.3).

Figure 3.3 illustrates the control diagram for the presented longitudinal model of the quadrotor. For this case study, the state partitioning is done as follows

$$^1x = \begin{bmatrix} \theta \\ p \end{bmatrix} \tag{3.4}$$

$$^2x = \begin{bmatrix} u \end{bmatrix} \tag{3.5}$$

28
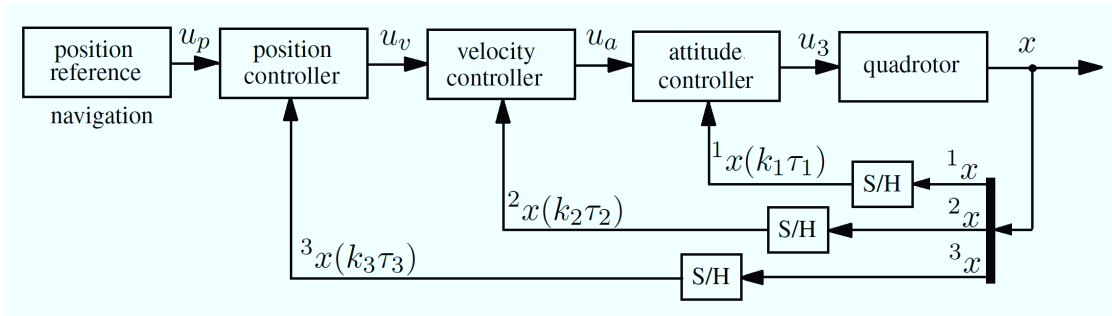
Figure 3.3: Quadrotor's control loops

$$^{3}x = \begin{bmatrix} X \end{bmatrix} \tag{3.6}$$

It is assumed that there is a stabilizing height controller that commands u_1. When the quadrotor's operation point is close to hover, u_1 is approximately equal to the vehicle's weight, and has very small changes to maintain the quadrotor's altitude constant. Since the attitude angles are close to zero, only a small proportion of the overall thrust, u_1 is not counteracting the weight of the vehicle. This becomes clear from equation (2.2). The previous analysis, based on the physics of the model, and the fact that the vehicle's mass, M is also constant, motivates the following assumption.

Assumption Q1: u_1/M is constant.

In this Chapter, dedicated to the kinematics control, the rotational dynamics are neglected, and the following assumption on the pitch angle is also made: Let us assume that the pitch angle can be controlled directly by the input u_a.

Assumption Q2: $\theta = u_a$

Please note that $u_a = \theta_{ref}$ and this assumption implies that the attitude dynamics are faster than the velocity and position dynamics; so one can assume that the reference is followed instantaneously by an attitude-tracking controller. Therefore, the dynamics of θ will be neglected at this stage. Later, in Chapter 4, this assumption will be removed, and an attitude-tracking controller will be designed and implemented. It will be shown that the

29

behavior of the closed-loop system under Assumption Q2 is a fairly good approximation of the original system when it is controlled using the proposed multi-rate approach. A linear controller will be designed for the velocity loop, and a Piecewise-Affine controller will be used for position.

3.2.1 Velocity control

In this subsection, the attitude reference u_a will be designed such that $u \to u_v$. Under Assumption Q2, equation (3.3) becomes:

$$\begin{cases} \dot{X} = u \\ \dot{u} = \dfrac{u_1}{M} \sin u_a \end{cases} \tag{3.7}$$

The dynamic equation of velocity, along the X axis, u, can now be linearized around zero for the purpose of designing a velocity controller. For a small angle, $\sin(u_a) \approx u_a$. Using this approximation, the velocity dynamics can be written as

$$\dot{u} = \frac{u_1}{M} u_a. \tag{3.8}$$

Now, assuming u_1/M constant (Assumption Q1), we design u_a in such a way that u tracks u_v (Figure 3.3). Note that u is sampled every τ_2 seconds, and its measured values are denoted by $^2x(k_2\tau_2)$. An appropriate gain k_v is chosen and the loop is closed by making

$$u_a = \frac{M}{u_1} k_v (u_v - {}^2x(k_2\tau_2)). \tag{3.9}$$

Then, the closed-loop system for velocity can be written as

$$\dot{u} = k_v (u_v - {}^2x(k_2\tau_2)). \tag{3.10}$$

If τ_2 is small compared to the system's time constant, $^2x(k_2\tau_2) \approx u(t)$, and the system (3.10) behaves as a continuous-time system for which the time-domain solution of can be

computed easily. It is found to be

$$u(t) = u_v + (u(t_0) - u_v)e^{-k_v t}, \tag{3.11}$$

which is an exponentially stable system. The settling time (t_s) of (3.11) is dependent on the parameter k_v, which can be chosen to make u converge to u_v much faster than τ_3. According to the 5% settling time criterion for linear systems in [57], the systems settles after approximaterly $3T$, where T is the system's time constant. For the case of equation (3.11), $t_s = 3/k_v$.

3.2.2 Position control

The quadrotor's position, X), is sampled and held every τ_3 seconds. These values are denoted by $^3x(k_3\tau_3)$ [see (3.6)]. The position control block commands u_v to be constant between two consecutive measurements of X. The constant value of u_v is selected such that X converges to u_p after τ_3 seconds. To achieve this, the commanded velocity is

$$u_v = \frac{u_p - {}^3x(k_3\tau_3)}{\tau_3}. \tag{3.12}$$

In practice, however, the vehicle's speed is limited, and cannot be larger than a known positive value $\overline{u_v}$. Hence, if the magnitude of the required velocity to reach u_p in τ_3 seconds is greater than $\overline{u_v}$, that limit value is commanded. Consequently,

$$u_v(s) = \begin{cases} -\overline{u_v} & \text{if} \quad s < -\overline{u_v} \\ s & \text{if} \quad |s| \leq \overline{u_v} \\ \overline{u_v} & \text{if} \quad s > \overline{u_v} \end{cases} \tag{3.13}$$

$$s = \frac{u_p - {}^3x(k_3\tau_3)}{\tau_3}. \tag{3.14}$$

Then, using **sat** to denote the standard saturation function,

$$u_v = \textbf{sat}\left[\frac{u_p - {}^3x(k_3\tau_3)}{\tau_3}\right], \tag{3.15}$$

and using (3.10), the closed loop system can then be rewritten as

$$
\begin{cases}
\dot{X} = u \\
\dot{u} = k_v \left(\mathbf{sat} \left[\dfrac{u_p - {}^3x(k_3\tau_3)}{\tau_3} \right] - {}^2x(k_2\tau_2) \right)
\end{cases}
\cdot
\tag{3.16}
$$

The relevance of the proposed control law becomes more evident when the sampling rate of the outer feedback loop is very low when compared to the time time constant k_v^{-1}, and verifies

$$
\tau_3 \gg \frac{3}{k_v}.
\tag{3.17}
$$
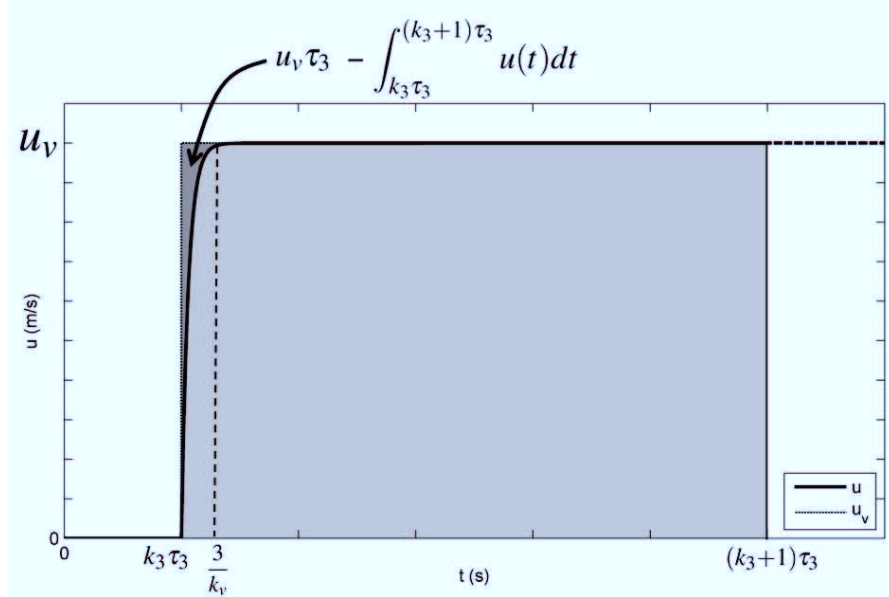
Figure 3.4: Quadrotor's velocity tracking

Figure 3.4 illustrates a typical velocity response of system 3.16 when 3.17 is verified. The dark grey area is the error in the approximation, which is small compared to the light gray area. This motivates the approximation made on (3.19). In Section 3.4 the stability analysis and velocity of convergence will be addressed.

The discrete dynamics for X can be written as

$$
X((k_3+1)\tau_3) = {}^3x((k_3+1)\tau_3) = {}^3x((k_3)\tau_3) + \int_{k_3\tau_3}^{(k_3+1)\tau_3} u(t)dt.
\tag{3.18}
$$

32

However, noting that u_v is constant in the interval $[k_3\tau_3, (k_3 + 1)\tau_3)$ and taking into account that u(t) reaches steady state very fast, then $u(t) \approx u_v$ during most of the time elapsed in the interval $[k_3\tau_3, (k_3 + 1)\tau_3)$ if 3.17 is true, and

$$\int_{k_3\tau_3}^{(k_3+1)\tau_3} u(t)dt \approx \int_{k_3\tau_3}^{(k_3+1)\tau_3} u_v dt = u_v\tau_3. \tag{3.19}$$

Therefore, we can write

$$\boxed{{}^3x((k_3 + 1)\tau_3) \approx {}^3x((k_3)\tau_3) + u_v\tau_3}. \tag{3.20}$$

3.2.3 Simulation results

The following simulations of the closed-loop system, were made using the proposed control approach. The HYCONS quadrotor parameters were used. The control task is to track a reference $u_p = 5m$. The selection of the samping period for u, τ_2, is based on the MicroStrain 3DX-GM IMU, that provides measurements at a rate of $76Hz$, and τ_3 is set to a large value ($10s$), to facilitate the illustration and emphasize the advantages of this control algorithm. The used simulation parameters are summarized in Table 3.1.

Parameter	Value	Units
u_1/M	25	g^{-1}
u_p	5	m
$\overline{u_v}$	0.2	m/s
τ_2	13.2	ms
τ_3	10	s
k_v	.32	
$X(0)$	0	m
$u(0)$	0	m/s

Table 3.1: Parameters for the quadrotor's kinematic control simulation

Figure 3.5 shows a plot of the obtained results. The quadrotor reaches the position reference after three position measurements, at $t = 30s$. It is clear from the plot that the position follows a straight line between two sampling periods due to the constant velocity reference that is given by the position controller. This fact is also evident in the plot of u,

where u_v is constant between the position sampling times. It can also be noted how fast u converges to u_v compared to τ_3, as it was predicted in equation (3.11). During the first two steps (from $t = 0$ to $t = 20$), the commanded velocity is constrained by the saturation, making $u = \overline{u_v}$. On the third measurement, the vehicle's position is about $1m$ away from the position reference ($X = 4m$); therefore the commanded velocity is equal to $0.1m/s$, in such way that it travels the required distance in the next $10s$. As the vehicle reaches the given reference after $30s$, the commanded velocity is made zero, allowing the quadrotor to stay in the commanded position. The pitch angle, commanded by u_a, has spikes whenever the velocity has to change, in order to produce the necessary acceleration to reach the speed reference.

3.3   Land rover

The land rover is modeled as a unicycle. Consider the following unicycle model,

$$
\begin{cases}
\dot{x} = v\cos(\psi) \\
\dot{y} = v\sin(\psi) \\
\dot{\psi} = au
\end{cases}
\tag{3.21}
$$

where

- x and y are the vehicle's coordinates with respect to an inertial reference frame,

- v is the unicycle's forward speed,

- ψ is the heading angle,

- a is the vehicle's rotational speed per input unit (constant), and

- u is the system's input.

Figure 3.6 shows an illustration of a unicycle with the most relevant parameters involved.

From (3.21) it is clear that the system is underactuated since it has three degrees of

34
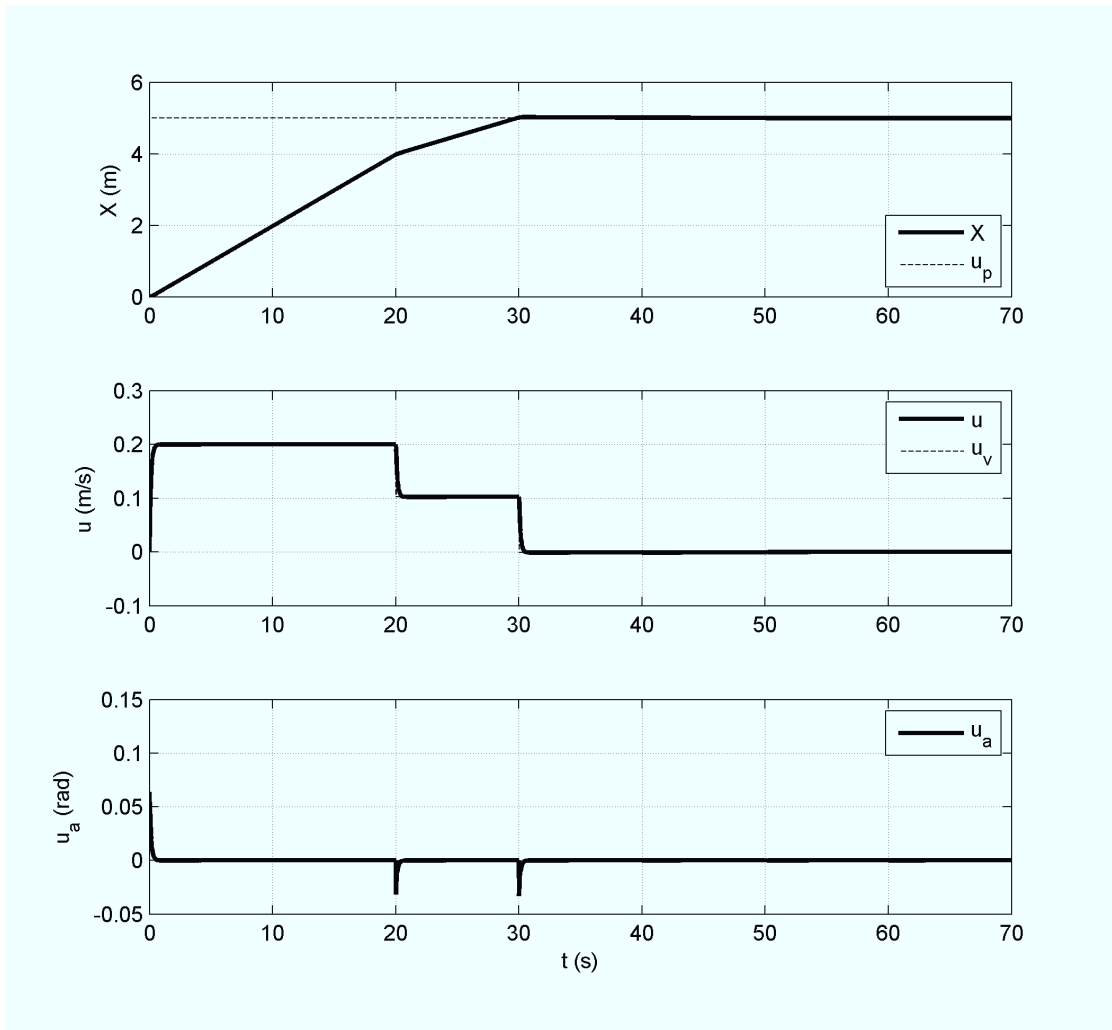
Figure 3.5: Simulation plots of the quadrotor's kinematic control

freedom and only one control input. A controller will be designed to follow the line $y = 0$. Hence, the vehicles' x position will not be shown in the equations from now on.

The proposed control strategy takes advantage of two facts:

- The rates of change in position are exclusively dependent on the heading angle and the velocity, which is constant.

- The heading angle dynamics are significantly faster than the position dynamics.
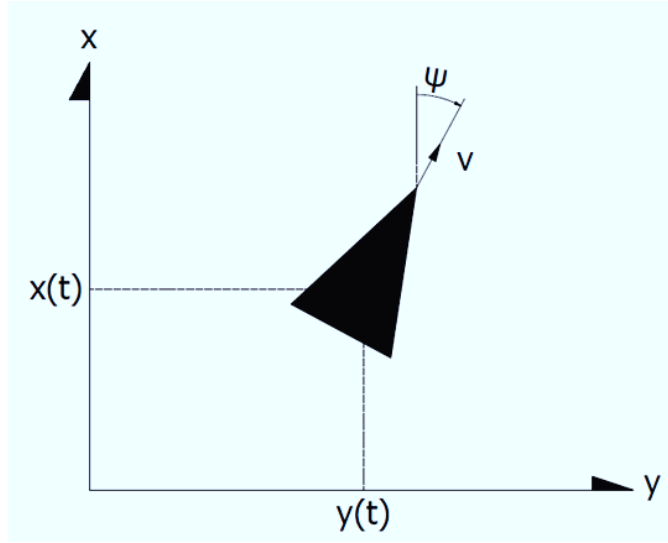
Figure 3.6: Illustration of a unicycle

From (3.21) it is possible to see that the velocity along the *y* axis does not have dynamics with respect to the heading angle, and the two variables are related by an algebraic equation. Therefore, it is possible to compute $\dot{y}$ based on ψ. Although the general block diagram can be applied, only two dynamical loops are really used. The control tasks are broken in two loops, each with a different sampling rate; an outer loop for position and an inner loop for the heading angle. Hence, two controllers are required: a position controller to compute the appropriate heading angle that yields the velocity that is necessary to lead the vehicle to a desired position or path, and another one to control the unicycle's orientation and follow the heading reference given by the outer control loop. Figure 3.7 illustrates the proposed control block diagram.

For this case study, the state partitioning is done as follows

$$^1x = \begin{bmatrix} \psi \end{bmatrix} \tag{3.22}$$

$$^2x = \begin{bmatrix} \dot{y} \end{bmatrix} \tag{3.23}$$

36
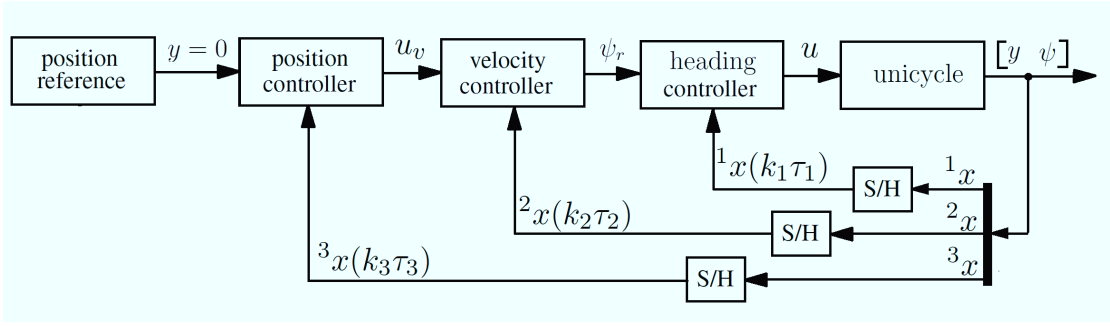
Figure 3.7: Unicycle's control loops.

$$^3x = \begin{bmatrix} y \end{bmatrix} \tag{3.24}$$

As it was mentioned in Section 3.2, this Chapter is dedicated to the kinematics control. Hence, the following assumption on the heading angle is made. Let us assume that ψ can be controlled directly by the input ψ_r. This is

Assumption U1: $\psi = \psi_r$

In Chapter 4, the assumption will be removed, and a heading controller to track the given reference will be used. It will be shown that the behavior of the closed-loop system under Assumption U1 is a good approximation of the original system when ψ is controlled using the proposed multi-rate approach.

3.3.1 Velocity control

In this subsection, the velocity control is addressed. Since there are no dynamics for $\dot{y}$ with respect to ψ, for this case study, the task is to finding an appropriate heading reference ψ_r such that $\dot{y} \to u_v$.

Under the Assumption U1, equation (3.21) becomes:

$$\dot{y} = v sin(\psi_r) \tag{3.25}$$

Since there are no dynamics involved in the velocity loop, by making $u_v = \dot{y}$, it is

37

possible to find the required heading angle such that the commanded velocity is achieved. We can write

$$u_v = v sin(\psi_r), \tag{3.26}$$

and solve for ψ_r to find

$$\psi_r = sin^{-1}\left(\frac{u_v}{v}\right). \tag{3.27}$$

3.3.2 Position control

In this subsection, the velocity reference u_v is designed such that the vehicle converges to the desired position reference. The objective chosen for this case study is following the straight line $y = 0$, hence u_v is designed such that $y \rightarrow 0$.

The position is measured every τ_3 seconds. The proposed control strategy aims at getting to $y = 0$ after one measurement and control step. This is done by making the magnitude of the velocity along the y axis constant between two sampling times and equal to the ratio of the measured position and the sampling period. This means that u_v, is

$$u_v = -\frac{^3x(k_3\tau_3)}{\tau_3}. \tag{3.28}$$

Replacing u_v in equation (3.27), one finds

$$\psi_r = sin^{-1}\left(-\frac{^3x(k_3\tau_3)}{v\tau_3}\right). \tag{3.29}$$

In practice, the maximum $\dot{y}$ is v. Hence, for this case study,

$$|\overline{u_v}| = \pm v \tag{3.30}$$

From 3.21, this occurs when $\psi = \pm\pi/2$. Evidently, this fact is considered in (3.31): if the vehicle's position in the y axis, $^3x(k_3\tau_3)$, is larger in magnitude than the distance that

38

can be covered between two consecutive sampling times, $v\tau_3$, the commanded heading angle is $\pm\pi/2$. Since sin^{-1} is defined for an argument in the interval $[-1,1]$, we use **sat** to denote the standard saturation and write

$$\psi_r = sin^{-1}\left[\textbf{sat}\left(\frac{-^3x(k_3\tau_3)}{v\tau_3}\right)\right] \tag{3.31}$$

Replacing (3.31) in (4.37) to obtain the closed-loop dynamics,

$$\dot{y} = vsin\left\{sin^{-1}\left[\textbf{sat}\left(\frac{-^3x(k_3\tau_3)}{v\tau_3}\right)\right]\right\} \tag{3.32}$$

yields

$$\dot{y} = v\textbf{sat}\left(\frac{-^3x(k_3\tau_3)}{v\tau_3}\right). \tag{3.33}$$

The discrete dynamics of the system can be written as

$$y((k_3+1)\tau_3) = y(k_3\tau_3) + \int_{k_3\tau_3}^{(k_3+1)\tau_3}\dot{y}(\tau)d\tau. \tag{3.34}$$

Note that ψ_r is constant between two consecutive sampling times, and so is $\dot{y}$ in consequence. By letting

$$\Delta = v\tau_3\textbf{sat}\left(\frac{-^3x(k_3\tau_3)}{v\tau_3}\right) \tag{3.35}$$

we can write the system's discrete dynamics as

$$y((k_3+1)\tau_3) = y(k_3\tau_3) + \Delta \tag{3.36}$$

In Section 3.4 the stability analysis and velocity of convergence will be discussed.

3.3.3 Simulation results

Simulations for the proposed multirate control algorithm were performed. Some simulation parameters were taken from the HYCONS Rover. The control task is to follow the

straight line $y = 0$. The used sampling period was $10s$. The used simulation parameters are summarized in Table 3.2.

Parameter	Value	Units
v	1	m/s
a	1	rad/s
τ_3	10	s
$y(0)$	15	m
$\psi(0)$	0	rad

Table 3.2: Simulation parameters for the unicyle's kinematic control

Figure 3.8 shows the obtained results. The vehicle reaches the position reference after two position measurements, at $t = 20s$. In the plot, it is evident that $y(t)$ follows a straight line during the time elapsed between two consecutive position measurements. This behavior comes from the fact that the velocity command is constant during each sampling period, and is only updated once a new position is measured. It is also clear from the plots that both the velocity along the y axis and the angle command ψ_r are constant during the ten seconds it takes for the measurement to be updated. During the first step (from $t = 0$ to $t = 10$), the commanded velocity is constrained by the saturation, making $u_v = -1$. After the first step, the vehicle's position is $5m$ away from $y = 0$; hence, the velocity command for the second step is $-5m/10s = -0.5m/s$. After the first two steps, the desired reference is reached, and the vehicle stays there, following the objective line $y = 0$. It is clear that after the desired position is reached, both the commanded velocity and heading angle are set to zero by the controller, making the vehicle stay in the line.

Figure 3.9 shows the phase plane plot of the system for y and $\dot{y}$ for several initial conditions. It is clear from the plot that the vehicle converge to the origin regardless of the initial starting conditions. Straight lines that are parallel to the y axis show the vehicle's constant velocity during the inter sampling times. Note also that the values for the constant velocities are equal to the ratio of the measured positions and the sampling time of 10s.
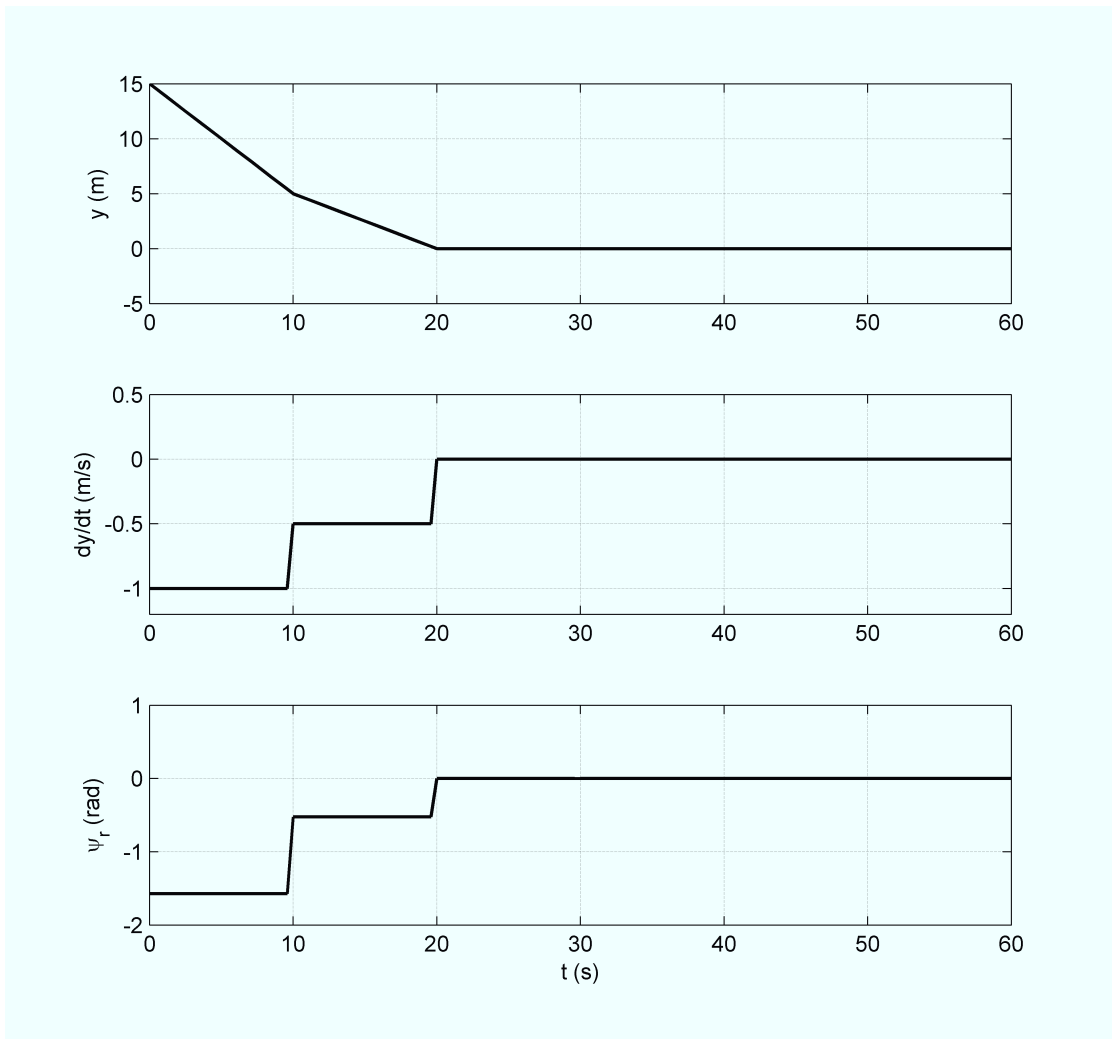
Figure 3.8: Kinematic control simulation of the unicycle

3.4 Stability analysis and velocity of convergence

This section presents the stability analysis and velocity of convergence of the proposed multirate control approach. The general system discussed in the first section of this Chapter is used for this purpose, and the analysis applies to both case studies. The two case studies presented in this chapter have a similar structure that allows splitting the control tasks in subsystems. Each subsystem, represented by a loop, can have a different sampling rate. The inner loops have the task of controlling an angle that will ultimately determine

41
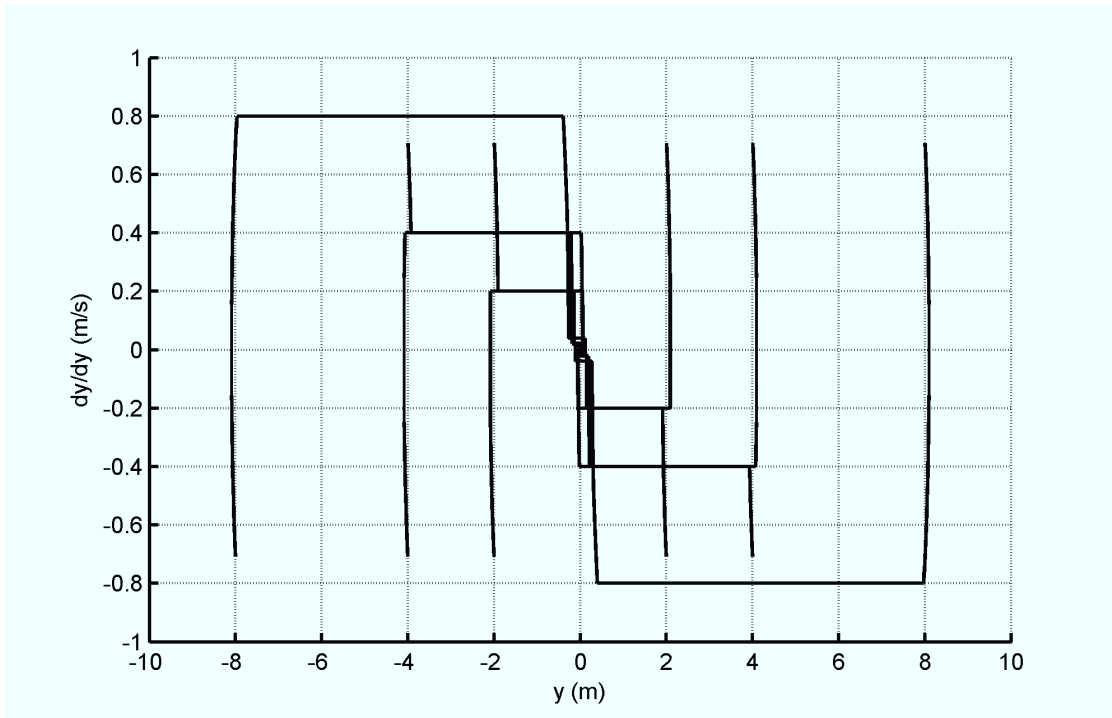
Figure 3.9: Phase plane plot of the unicycle's kinematic control

the velocity along an axis of displacement.

In the case of the unicycle, the forward velocity is considered constant, and a heading angle changes the proportion of that speed along the y axis. In the case of the quadrotor, the velocity is controlled indirectly by the attidude angles. The angles do not describe the velocity along the axes of displacement directly, but indicate the orientation of the thrust produced by the motors. The velocity is controlled by setting an appropriate behavior to the attitude angles, such that the commanded velocity is reached. Once the velocity is controlled, the vehicle can track waypoints using the proposed algorithm.

The main stability result is now stated.

Theorem: *The position trajectories of systems (3.7) and (4.37) converge to the value u_p after $n+1$ position sampling periods.*

Proof:

Depending on the measured distance between the vehicle at $t = k_3 \tau_3$ and the position

42

reference u_p, three cases can occur:

Case 1: $^3x(k_3\tau_3) > u_p + \overline{u_v}\tau_3$

This implies that

$$\frac{u_p - {}^3x(k_3\tau_3)}{\tau_3} < -\overline{u_v}. \tag{3.37}$$

Hence, according to equations (3.14) and (3.13) in the case of the quadrotor and (3.30) for the unicycle, $u_v = -\overline{u_v}$. Then, from (3.20) and (3.36),

$$^3x(k_3\tau_3) = {}^3x((k_3+1)\tau_3) + \overline{u_v}\tau_3. \tag{3.38}$$

Replacing $^3x(k_3\tau_3)$ in inequality (3.37),

$$\begin{aligned} {}^3x((k_3+1)\tau_3) + \overline{u_v}\tau_3 &> u_p + \overline{u_v}\tau_3 \\ {}^3x((k_3+1)\tau_3) &> u_p \end{aligned} \tag{3.39}$$

Also, from 3.20, and since $\overline{u_v}\tau_3$ is strictly positive,

$$^3x((k_3+1)\tau_3) < {}^3x(k_3\tau_3). \tag{3.40}$$

In consequence,

$$\boxed{u_p < {}^3x((k_3+1)\tau_3) < {}^3x(k_3\tau_3)} \tag{3.41}$$

Case 2: $^3x(k_3\tau_3) < u_p - \overline{u_v}\tau_3$

Following the same analysis as in Case 1, it is clear that $u_v = \overline{u_v}$, implying that

$$^3x(k_3\tau_3) = {}^3x((k_3+1)\tau_3) - \overline{u_v}\tau_3. \tag{3.42}$$

Replacing $^3x(k_3\tau_3)$ in inequality (3.37),

$$^3x((k_3+1)\tau_3) - \overline{u_v}\tau_3 \quad < u_p - \overline{u_v}\tau_3$$
$$^3x((k_3+1)\tau_3) \qquad < u_p. \tag{3.43}$$

Since $\overline{u_v}\tau_3$ is strictly positive, it is also clear that

$$^3x((k_3+1)\tau_3 > \,^3x(k_3\tau_3). \tag{3.44}$$

It yields

$$\boxed{u_p > \,^3x((k_3+1)\tau_3) > \,^3x(k_3\tau_3)} \tag{3.45}$$

Case 3: $u_p - \overline{u_v}\tau_3 \leq \,^3x(k_3\tau_3) \leq u_p + \overline{u_v}\tau_3$

Under this condition, from equations (3.14) and (3.13), it is found that

$$u_v = \frac{u_p - \,^3x(k_3\tau_3)}{\tau_3}. \tag{3.46}$$

Implying that

$$^3x((k_3+1)\tau_3) = \,^3x(k_3\tau_3) + \frac{u_p - \,^3x(k_3\tau_3)}{\tau_3}\tau_3, \tag{3.47}$$

therefore,

$$\boxed{^3x((k_3+1)\tau_3) = u_p} \tag{3.48}$$

Equation (3.48) shows that if $^3x(k_3\tau_3)$ is contained in the region of Case 3, x_1 converges to u_p after only one sampling period. It will now be shown that if $x_1(0)$ is any finite value, x_1 will converge to the region of Case 3 in a finite and predictable number of sampling periods. This will prove that the system converges to $x_1 = u_p$ in a finite number of steps, regardless of the starting position.

Let $n \in Z^+$ be an arbitrary number of sampling periods and $^3x(n\tau_3)$ the vehicle's position after $n\tau_3$ seconds. From (3.38) and (3.42), it is evident that $^3x(k_3\tau_3)$ follows

an arithmetic sequence in the regions of Case 1 and Case 2, respectively. An arithmetic sequence has the form

$$^3x(n\tau_3) = {}^3x(0) + n\Delta. \tag{3.49}$$

An arithmetic sequence grows in uniform steps towards positive infinity if Δ is positive, or grows towards negative infinity if Δ is negative.

For Case 1, x_1 will decrease until $u_p < x_1(n\tau_3) \leq u_p + \overline{u_v}\tau_3$, getting in the region of Case 3. Denoting $\lceil \cdot \rceil$ as the smallest positive number greater or equal than its argument, and making $^3x(n\tau_3) = u_p + \overline{u_v}\tau_3$, from (3.49) and (3.38), the number of required sampling periods to reach the region of Case 3 is

$$n = \left\lceil \frac{x_1(0)}{\overline{u_v}\tau_3} - 1 \right\rceil \tag{3.50}$$

Following the same reasoning, for Case 2, x_1 will increase in uniform steps until $u_p > x_1(n\tau_3) \geq u_p - \overline{u_v}\tau_3$, getting also in the region of Case 3. From (3.49) and (3.42) and making $^3x(n\tau_3) = u_p - \overline{u_v}\tau_3$,

$$n = \left\lceil -\frac{x_1(0)}{\overline{u_v}\tau_3} - 1 \right\rceil \tag{3.51}$$

As shown in (3.48), once x_1 reaches the region of Case 3, it converges to u_p in one additional sampling period. Furthermore, (3.15) and (3.9) shows that if $x_1 = u_p$, also $u_v = u_a = 0$; therefore, $x_2 = x_3 = 0$. This proves that the system converges to u_p and remains there after $n+1$ sampling periods. $\blacksquare$

Chapter 4

Dynamics Control and Experimental Results

This chapter discusses the dynamics control of the two case studies introduced in Chapter 3 using the proposed multirate control technique. Each system model is analyzed and simulated, considering both its kinematics and dynamics. In addition to this, experimental results obtained with the HYCONS Quadrotor and the HYCONS Rover are presented. The results of this chapter clearly show that Assumptions Q2 and U1 are reasonable from a practical point of view. It is shown that for most of the simulation time, Assumptions Q2 and U1 are valid, and the short transient periods of time when they are not valid do not have any influence in the steady state behavior of the closed-loop system. To motivate future extensions of the work presented in this thesis, a brief analysis of the unicycle's control model using singular perturbations theory is discussed at the end of this chapter.

4.1   Quadrotor Helicopter

In the first part of this section, the dynamics component of the proposed multirate control technique for the case of the HYCONS quadrotor helicopter is discussed. The dynamics control, which is done in the attitude loop (see Figure 4.1), has the objective of making
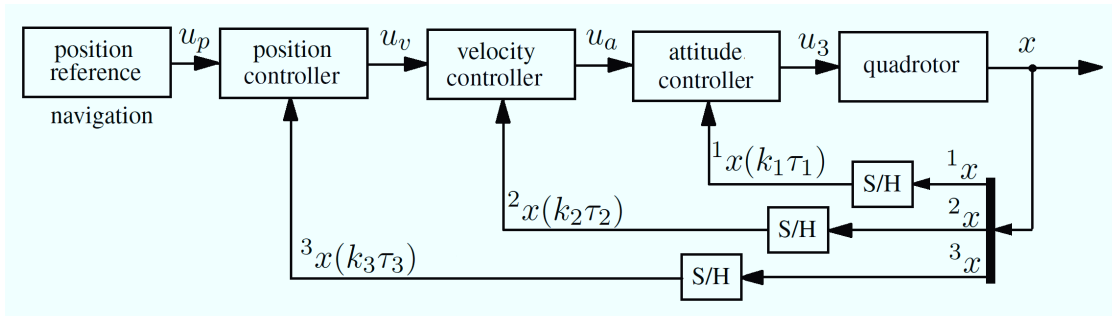
Figure 4.1: Quadrotor's control loops

the quadrotor track the reference attitude angle given by the kinematics control. Later in this section, the complete control system, including both dynamics and kinematics, is analyzed and simulated. Finally, experimental results obtained with the HYCONS quadrotor helicopter are presented. Figure 4.1 shows the control blocks diagram that was introduced in Chapter 3, to facilitate the reading of this section.

The same state partitioning used in Chapter 3 is used again in this chapter, i.e.,

$$ {}^1x = \begin{bmatrix} \theta \\ p \end{bmatrix} \tag{4.1} $$

$$ {}^2x = \begin{bmatrix} u \end{bmatrix} \tag{4.2} $$

$$ {}^3x = \begin{bmatrix} X \end{bmatrix} \tag{4.3} $$

Next, the attitude-tracking controller is designed, and the analysis of the rest of the system is done considering the inner loop's dynamics.

4.1.1 Attidude control

The attitude angles were assumed to be directly set by the given reference in Chapter 3 for the pitch loop. The other loops are designed in the same manner. This reference angle, denoted by u_a was assumed to be equal to θ in Assumption Q2. Now, this assumption is

no longer used, and an attitude angle tracking controller is designed. It will be later shown that the system behaves very similarly when the assumption is made and when the angle is tracked by the attitude controller.

As stated before, three different controllers per horizontal axis (X, Y) must be designed to stabilize the system using the proposed multi-rate control technique. Every time a new position sampling is made, the position control computes the constant speed required to get to the reference position after $\overline{\tau_3}$ seconds. If the magnitude of this required speed is greater than the vehicle's maximum speed $|\overline{u_v}|$, this maximum speed is commanded. The velocity controller commands the attitude angles so that the speed given as reference by the position controller is achieved and maintained.

Remark: *In principle, intuition leads to think that as long as the angles converge fast enough to the given reference u_a, any controller can be implemented to track the attitude reference and the overall system will still be stable and converge to the commanded position.*

Attitude angles are small during non-aggressive maneuvers. Hence, linear controllers can be used for the attitude loop. Following the approach used in Chapter 3, one of the axis of displacement is isolated to help the illustration of the proposed multirate control technique. From equation (3.3), the dynamics of the attitude angle are

$$
\begin{cases}
\dot{\theta} = p \\
\dot{p} = u_3/Iyy
\end{cases}
\tag{4.4}
$$

We now design u_3 using a pole-placement procedure in such a way that θ tracks its reference, u_a with an overshoot of 1% and a settling time of $0.25s$.

As stated before, θ and p are sampled with a period of τ_1. The sampled sub state vector ^1x is denoted by

$$^1x(k_1\tau_1) = \begin{bmatrix} \theta(k_1\tau_1) \\ p(k_1\tau_1) \end{bmatrix}.$$ (4.5)

A state feedback controller is designed for the pitch control as

$$u_3 = k_a(\vec{u}_a - {^1x}(k_1\tau_1))$$ (4.6)

where

$$k_a = \begin{bmatrix} 1 & 0.09 \end{bmatrix}$$ (4.7)

and

$$\vec{u}_a = \begin{bmatrix} u_a \\ 0 \end{bmatrix}$$ (4.8)

Hence, the closed-loop attitude-tracking system is

$$\begin{cases} \dot{\theta} = p \\ \dot{p} = \dfrac{k_a}{Iyy}(\vec{u}_a - {^1x}(k_1\tau_1)) \end{cases}$$ (4.9)

Figure 4.2 shows a simulation of the designed attitude-tracking controller in equation (4.9). Table 4.1 summarizes the parameters used in the simulation. The time-response follows the design criteria; the settling time is $0.25s$ and the overshoot is about 1%.

Parameter	Value	Units
τ_1	13.2	ms
$1/Iyy$	322	kg/m^2
u_a	$\pi/4$	rad
$x_3(0)$	0	rad
$x_4(0)$	0	rad/s

Table 4.1: Simulation parameters for the attitude-tracking controller simulation

The used sampling period τ_1 was chosen to be equal to the one provided by the implemented sensor and network ($76Hz$), which yields a sampling period of $13.2ms$. It is now proven that the attitude stabilization system is stable for this sampling rate.
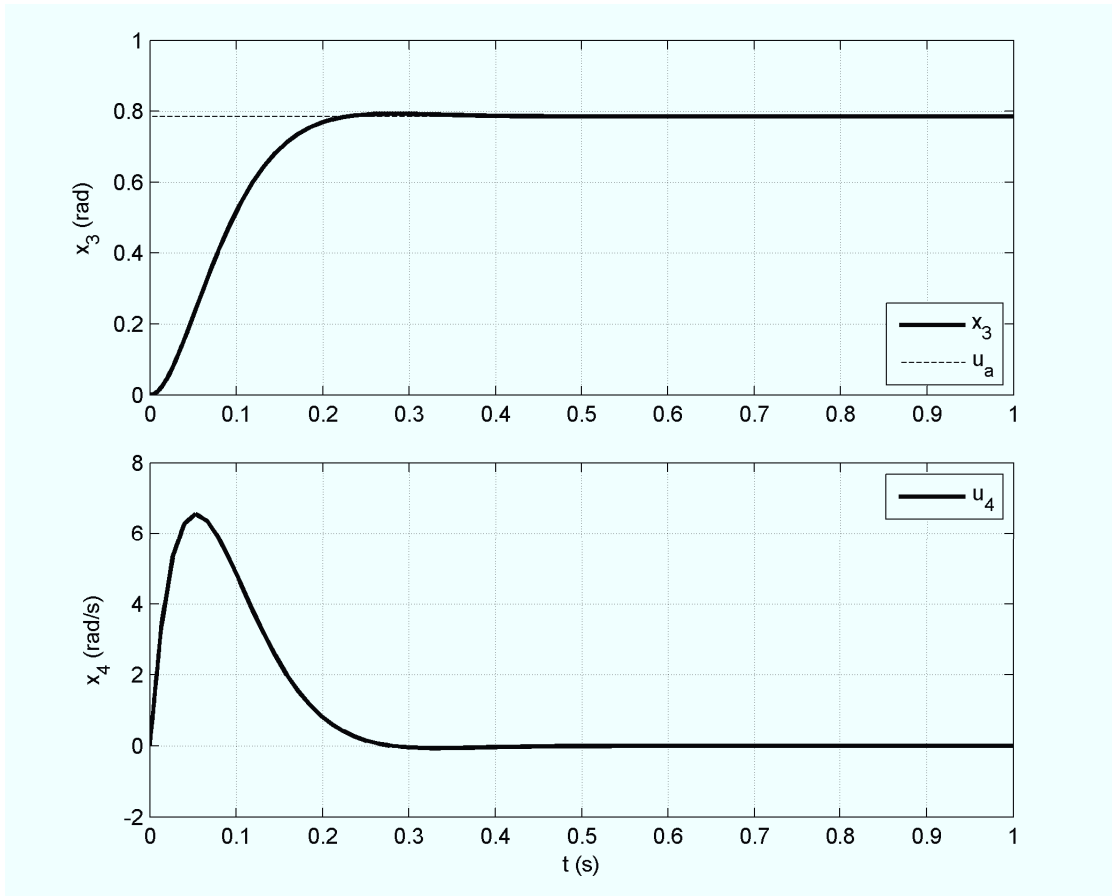
Figure 4.2: Attitude-tracking controller simulation

The attitude-tracking control is a linear system that can be written in the form

$$\dot{x}(t) = Ax(t) + Bu(t), \tag{4.10}$$

For which a continuous-time linear controller of the form

$$u(t) = Kx(t) \tag{4.11}$$

can be designed.

Assumption 4.1.1. *The measurements for computing the control input are taken in a*

sample-and-hold fashion. Therefore, the control input can be rewritten as

$$u(t) = Kx_{t_n}, \text{ for } t \in [t_n, t_{n+1}),$$ (4.12)

where t_n and t_{n+1}, $n \in \mathbb{N}$, are two consecutive sampling times, and $x_{t_n} = x(t_n)$.

We denote the time elapsed since the last sampling instant by

$$\rho(t) = t - t_n, \text{ for } t \in [t_n, t_{n+1}),$$ (4.13)

and the longest interval between two consecutive sampling times by τ, i.e,

$$\tau = \sup_{n \in \mathbb{N}}(t_{n+1} - t_n).$$ (4.14)

We denote the $m \times m$ identity matrix by I_m.

The next theorem follows from the results of [59], and provides a set of linear matrix inequalities which guarantee that the sampled-data linear system asymptotically converges to the origin.

Theorem 4.1.1. *Consider the closed-loop sampled-data linear system defined in (4.10) and (4.12) with sampling intervals smaller than τ. The system is asymptotically stable to the origin if there exist symmetric positive definite matrices P, R, and X, and matrix N with appropriate dimensions, satisfying*

$$\Psi + \tau(M_1 + M_2) < 0$$ (4.15)

$$\begin{bmatrix} \Psi + \tau(M_2 + M_3) & \tau N \\ \tau N^T & -\tau R \end{bmatrix} < 0$$ (4.16)

where

$$\Psi = \begin{bmatrix} A^T \\ K^T B^T \end{bmatrix} \begin{bmatrix} P & 0 \end{bmatrix} + \begin{bmatrix} P \\ 0 \end{bmatrix} \begin{bmatrix} A & BK \end{bmatrix}$$

$$-\begin{bmatrix} I_{n_x} \\ -I_{n_x} \end{bmatrix} X \begin{bmatrix} I_{n_x} & -I_{n_x} \end{bmatrix} - \begin{bmatrix} I_{n_x} \\ -I_{n_x} \end{bmatrix} N^T - N \begin{bmatrix} I_{n_x} & -I_{n_x} \end{bmatrix},$$

$$M_1 = \begin{bmatrix} A^T \\ K^T B^T \end{bmatrix} X \begin{bmatrix} I_{n_x} & -I_{n_x} \end{bmatrix} + \begin{bmatrix} I_{n_x} \\ -I_{n_x} \end{bmatrix} X \begin{bmatrix} A & BK \end{bmatrix},$$

$$M_2 = \begin{bmatrix} A^T \\ 0 \end{bmatrix} R \begin{bmatrix} A & 0 \end{bmatrix},$$

$$M_3 = \begin{bmatrix} 0 \\ K^T B^T \end{bmatrix} N^T + N \begin{bmatrix} 0 & BK \end{bmatrix}.$$

The proof of this theorem can be found in [59]. Based on Theorem 4.1.1, the problem of finding the longest interval between two consecutive sampling times that preserves asymptotic stability is formulated as

Problem 4.1.1.

$$maximize \ \ \tau$$

$$subject \ to \ \ P > 0, \ R > 0, \ X > 0, \ (4.15) - (4.16).$$

We denote the solution of Problem 4.1.1 by $\tau_{\max}$. Using the system's characteristics, τ_{max} is found to be 154ms.

This result, further explained in [60] is based on a Lyapunov-Krasovskii functional. The found upper bound for the maximum allowable sampling period was found to be 154ms, which is far higher than 13.16ms. Therefore, stability of the attitude loop is guaranteed (see [60] for more details).

Now, with this attitude-tracking controller, the velocity controller shown in Chapter 3 can be implemented, no longer using the Assumption Q2, and validating that this assumption is reasonable form a practical point of view. The velocity and position controllers that were designed in Chapter 3 are analyzed in the following subsections, taking into account the attitude angle dynamics.

4.1.2 Velocity control

The same velocity controller that was designed in Chapter 3 is now implemented in model
(3.3), considering the attitude dynamics. The velocity controller that was shown in equation (3.9) is used:

$$u_a = \frac{M}{u_1} k_v (u_v - {}^2x(k_2 \tau_2)). \tag{4.17}$$

Using (4.6), the model described in equation (3.3) is transformed into

$$
\begin{cases}
\dot{X} = u \\
\dot{u} = u_1/M \sin \theta \\
\dot{\theta} = p \\
\dot{p} = \frac{k_a}{Iyy} \left\{ \begin{bmatrix} \frac{M}{u_1} k_v (u_v - {}^2x(k_2 \tau_2)) \\ 0 \end{bmatrix} - {}^1x(k_1 \tau_1) \right\}
\end{cases}
\tag{4.18}
$$

where k_a is given by equation (4.7) and ${}^1x(k_1 \tau_1)$ and ${}^2x(k_2 \tau_2)$ are given by (4.1, 4.2).

The velocity-tracking simulation results are shown in subsection 4.1.4, together with the attitude and position tracking. It will now be shown that the system converges to u_p.

4.1.3 Position control

As in the previous subsection, the position controller that was discussed and designed in Chapter 3 is now implemented in model (3.3), considering the dynamics of the attitude angle. Replacing u_v in (4.18) by the velocity controller shown in equation (3.15), the closed-loop model takes the form

$$
\begin{cases}
\dot{X} = u \\[2mm]
\dot{u} = u_1/M\sin\theta \\[2mm]
\dot{\theta} = p \\[2mm]
\dot{p} = \dfrac{k_a}{Iyy}\left\{\left[\dfrac{M}{u_1}k_v\left[\mathbf{sat}\left(\dfrac{u_p - {}^3x(k_3\tau_3)}{\tau_3}\right) - {}^2x(k_2\tau_2)\right]\right] - {}^1x(k_1\tau_1)\right\}
\end{cases}
\tag{4.19}
$$

where u_p is desired position reference. Equation (4.19) is the model of a PWA control system for which the tools presented in [62] could be extended in future work and then used to analyze stability. Note that the input u_3 to θ takes an interesting form due to the different rates at which the state measurements are made. The three portions of the state are interacting in the same expression, and being updated at different rates. The inner round brackets, where the position input is computed, is updated every τ_3 seconds. Until the next position measurement is done, the velocity commands are computed in the square bracket at a rate of $1/\tau_2 Hz$. In turn, this velocity input sets the reference to the attitude-tracking controller, which is computed every τ_1 seconds. The combination of these three inputs at different rates, produces the necessary commands to motors 2 and 4, so that the quadrotor's pitch angle envelope has an appropriate shape that makes the vehicle track a given position reference u_p in the X axis. The simulation results are shown in the next subsection.

4.1.4 Simulation results

System (4.19) was simulated using the parameters shown in Table 4.2. Both dynamics and kinematics are considered in this simulation. The Assumption Q2, made on Chapter 3 for the attitude angle is removed, and the attitude-tracking controller discussed in Subsection 4.1.1 is used instead. As in Chapter 3, the position sampling period (τ_3) is 10s and the given position reference $u_p = 5m$. The sampling period for ${}^2x$ and ${}^1x$ is again based on MicroStrain 3DX-GM IMU, $\tau_2 = \tau_3 = 13.2ms$.
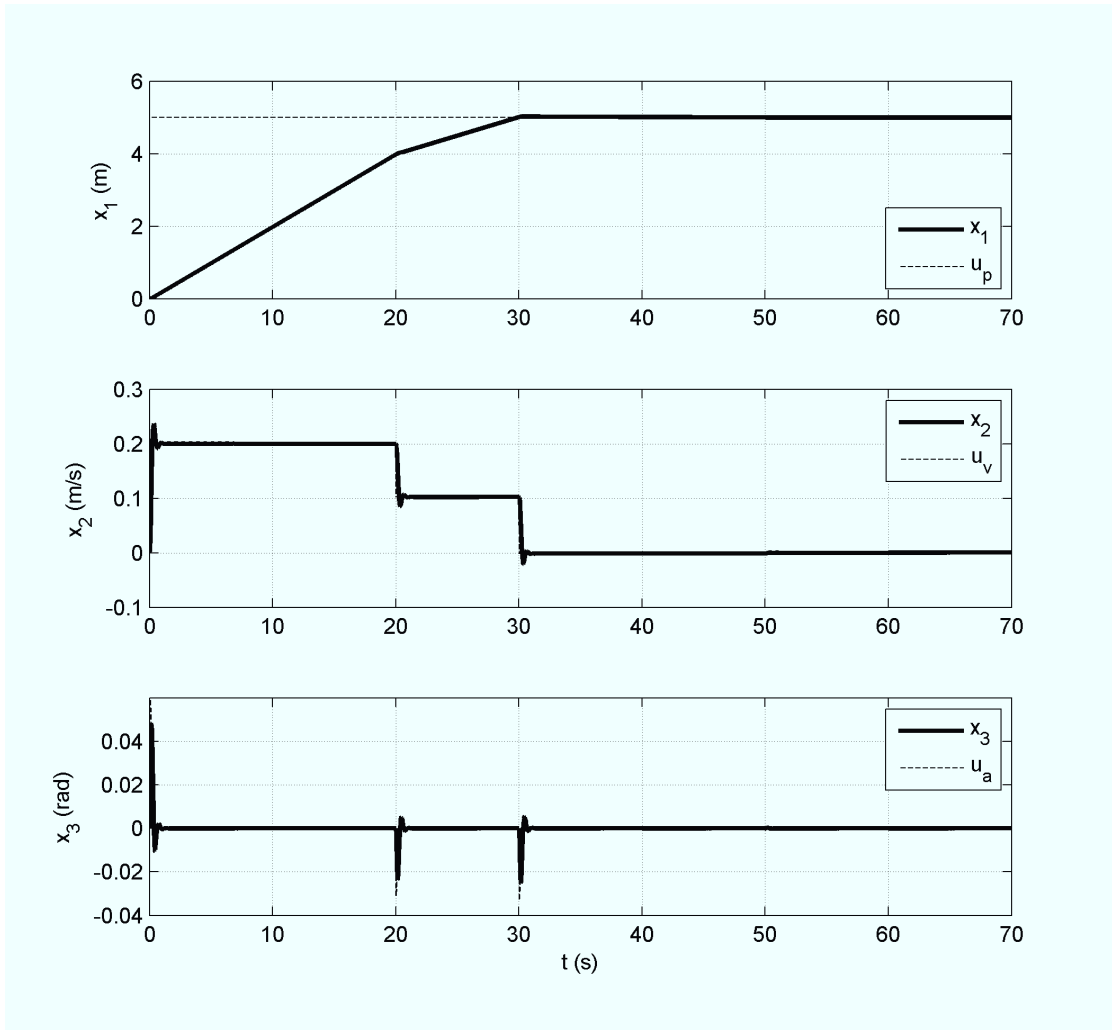
Figure 4.3: Dynamics control simulation of the HYCONS quadrotor model

The obtained results are shown in Figure 4.3. As in Figure 3.5, The quadrotor reaches the given position reference in $3\tau_3$ seconds, at $t = 30s$. The trajectory described by X is a straight line between two sampling periods due to the constant velocity reference that is given by the position controller. It can be noted that the velocity is tracked as fast as in the kinematics simulation shown in Chapter 3, although the angle is no longer assumed to be directly accessible as a control input, and an attitude-tracking controller is used instead. This confirms the effectiveness of the proposed multirate control technique and the fact that Assumption Q2 is reasonable from a practical point of view. Refer to Figure 3.5

55

Parameter	Value	Units
u_1/M	25	g^{-1}
$1/Iyy$	322	m^2/g
u_p	5	m
$\overline{u_v}$	0.2	m/s
τ_1	13.2	ms
τ_2	13.2	ms
τ_3	10	s
k_v	.32	
$X(0)$	0	m
$u(0)$	0	m/s
$\theta(0)$	0	rad
$p(0)$	0	rad/s

Table 4.2: Parameters for the quadrotor's dynamics control simulation

to verify the similarity of the two responses.

4.1.5 Experimental results

Figure 4.4 shows some experimental results obtained for the attitude stabilization control loop. The plot shows the attitude angles and its rates of change during a short take-off, hover and land flight. The roll and pitch angle references were set to zero; the yaw angle's rate of change was stabilized to zero by adding a damping input, since the magnetometer implemented in the UAV does not provide reliable information indoors, due to the strong electromagnetic interference that is present inside a building. It is evident from the plots that the attitude angles are stabilized around zero, with small oscillations of about $\pm 2deg$. Although some small oscillations are observed, the system remains stable during the maneuver.

Due to technical limitations, the presented results are preliminary, and only show the performance of the attitude control loop. The validation of the whole multirate control technique is proposed as future work. For this purspose, new equipment must be used to track the quadrotor's position in space with a good reliability, precision and repeatability. The acquisition of such equipment is being studied.
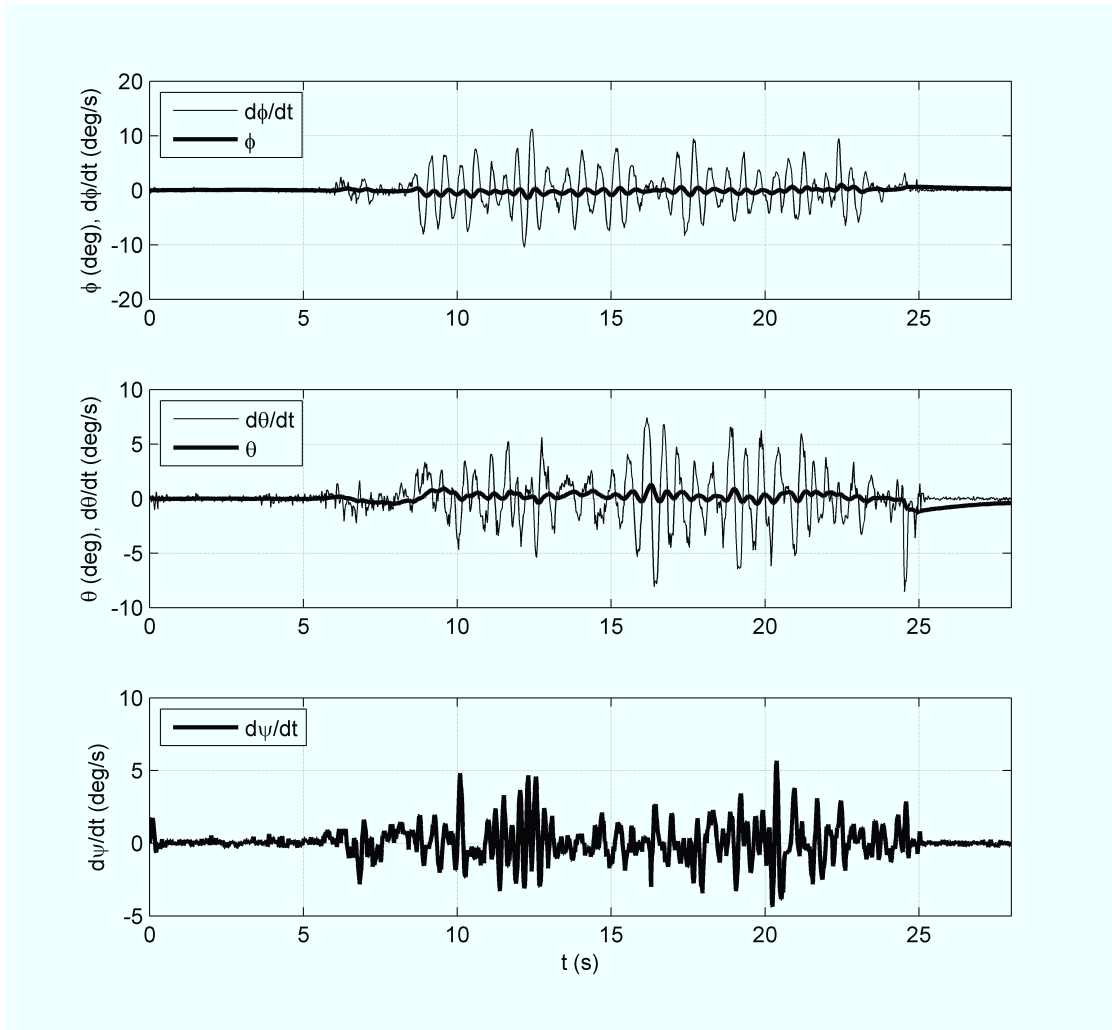
Figure 4.4: Experimental results obtained with the HYCONS Helicopter

4.2 Unicycle

The first part of this section addresses the rotational dynamics control of the unicycle. This component of the vehicle's control, is done in the inner loop of the proposed multirate system. This component has the task of making the heading angle track the reference signal that is given by the velocity controller. Later in this section, the analysis of the velocity and position loops is made, considering the rotational dynamics and the respective simulations are presented. It will be shown that the behavior of the system under the mentioned assumption is very similar to the one without the assumption, where the heading

angle reference is tracked by a controller. Finally, experimental results obtained with the HYCONS rover are presented.

The same partitioning of the state vector that was used in Chapter 3 is considered here:

$$^{1}x = \begin{bmatrix} \psi \end{bmatrix} \tag{4.20}$$

$$^{2}x = \begin{bmatrix} \dot{y} \end{bmatrix} \tag{4.21}$$

$$^{3}x = \begin{bmatrix} y \end{bmatrix} \tag{4.22}$$

The heading-tracking control is now addressed.

4.2.1   Heading angle tracking control

In Chapter 3, the heading angle, ψ, was assumed to be directly set by the reference ψ_r in Assumption U1. This is now removed, and a heading-tracking controller is designed and implemented instead. In subsection 4.2.4 it will be shown that the response is very similar in the cases when the assumption is made and when the heading controller is used.

Considering only the rotational dynamics of equation (3.21),

$$\dot{\psi} = au. \tag{4.23}$$

Using a state feedback controller, and noting that the sampled values of ψ are $^{1}x(k_1\tau_1)$, we make

$$u = k_\psi(\psi_r - {}^{1}x(k_1\tau_1)), \tag{4.24}$$

where ψ_r is the reference given to the inner control loop and k_ψ is an appropriate feedback gain. Using (4.24), equation 4.23 can be rewritten as

$$\dot{\psi} = ak_{\psi}(\psi_r - {}^1x(k_1\tau_1)) \tag{4.25}$$

which is a heading-tracking linear controller. The model of the unicycle, including the heading-tracking control rotational dynamics in (4.25), can then be written as

$$\begin{cases} \dot{y} = v\sin(\psi) \\ \dot{\psi} = ak_{\psi}(\psi_r - {}^1x(k_1\tau_1)) \end{cases} \tag{4.26}$$

The velocity control is addressed in the next subsection, and the heading angle reference, ψ_r is designed.

4.2.2 Velocity control

As discussed in section 3.3.1, the velocity loop does not have dynamics with respect to the rotational dynamics. The exact same relationship found in Chapter 3 is used here to compute the heading reference ψ_r based on the position control output u_v. This is

$$\psi_r = \sin^{-1}\left(\frac{u_v}{v}\right). \tag{4.27}$$

Hence, the model (4.26) becomes

$$\begin{cases} \dot{y} = v\sin(\psi) \\ \dot{\psi} = ak_{\psi}\left[\sin^{-1}\left(\frac{u_v}{v}\right) - {}^1x(k_1\tau_1)\right]. \end{cases} \tag{4.28}$$

In the next subsection, the input to system (4.28), u_v, is designed.

4.2.3 Position control

In this subsection, the analysis addressed in Chapter 3 is extended, considering the rotational dynamics of the unicycle. It was found that the velocity reference that is required for y to converge to zero after τ_3 seconds is

$$u_v = \frac{-{}^3x(k_3 \tau_3)}{\tau_3}.$$ (4.29)

Thus, the heading reference, according to equation (3.27) is

$$\psi_r = sin^{-1}\left[\mathbf{sat}\left(\frac{-{}^3x(k_3 \tau_3)}{v\tau_3}\right)\right]$$ (4.30)

and the model takes the form

$$\begin{cases} \dot{y} = vsin(\psi) \\ \dot{\psi} = ak_\psi \left\{ sin^{-1}\left[\mathbf{sat}\left(\frac{-{}^3x(k_3 \tau_3)}{v\tau_3}\right)\right] - {}^1x(k_1 \tau_1) \right\} \end{cases}$$ (4.31)

Equation (4.31) is the model of a PWA control system. It is worth noting the form that the input u takes here due to the different sampling rates that are present in the control system. The two partitions of the state space that are being measured are updated at different rates. The expression inside the curly brackets is updated every τ_1 seconds, based on the most recent value of ${}^3(k_3 \tau_3)$, that is only updated every τ_3 seconds and held constant until a new measurement is made.

These two inputs that are being updated at different rates are combined in such way that u is commanded to produce a heading angle envelope that makes the unicycle follow the straight line $y = 0$. Some simulation results are presented in the next subsection.

4.2.4   Simulation results

The system (4.31) was simulated to test the performance of the proposed multirate control technique. For those parameters that are common to the simulations in Chapter 3 and the one presented in this section, the same values are used. Table 4.3 summarizes the parameters used in the simulation. As stated before, the control task is to follow the straight line $y = 0$.

The obtained simulation results are shown in Figure 4.5. The unicycle converges to $y = 0$ after two position measurement periods; this is, $t = 20s$. In a very similar way to what

Parameter	Value	Units
v	1	m/s
a	1	rad/s
τ_1	0.04	s
τ_3	10	s
$y(0)$	15	m
$\psi(0)$	0	rad

Table 4.3: Simulation parameters for the unicyle's dynamics control

was shown in the kinematic control simulation results, the trajectory of $y(t)$ between two consecutive sampling times is a straight line, indicating that the velocity is constant. This fact is evident in the plot of $\dot{y}$, where the given reference is constant and the state tracks it in a small portion of τ_3. Note that in this simulation, where the rotational dynamics are included, the angle is no longer assumed to be directly accessible as input. Instead, a heading-tracking controller generates the appropriate signal u such that ψ converges fast to ψ_r. It is possible to see in the plot that the time it takes for ψ to converge to ψ_r is very small compared to τ_3, because of the difference in speed of the different state variable's dynamics. This shows the efficiency of the proposed multirate control technique. It is also possible to note that during from $t = 0$ to $t = 10$, the commanded velocity is kept constrained by the saturation, hence $u_v = -1$. The vehicle's position is $5m$ away from $y = 0$ in $t = 20s$; therefore, the velocity command for the second step is $-5m/10s = -0.5m/s$. After the first two steps, the desired reference is reached, and the vehicle stays there, following the objective line $y = 0$. It is clear that after the desired position is reached, both the commanded velocity and heading angle are set to zero by the controller, making the vehicle stay in the line.

A phase plane plot of the system is shown in Figure 4.6 for y and $\dot{y}$. Several initial conditions are considered. Similarly to what was shown in the phase plane plot in Chapter 3, the vehicle converges to the origin regardless of the initial starting conditions. If Figure 4.6 is carefully compared to Figure 3.9, small differences can be found in the shape of the trajectories. This small differences are caused by the short time it takes for $\dot{y}$ to converge
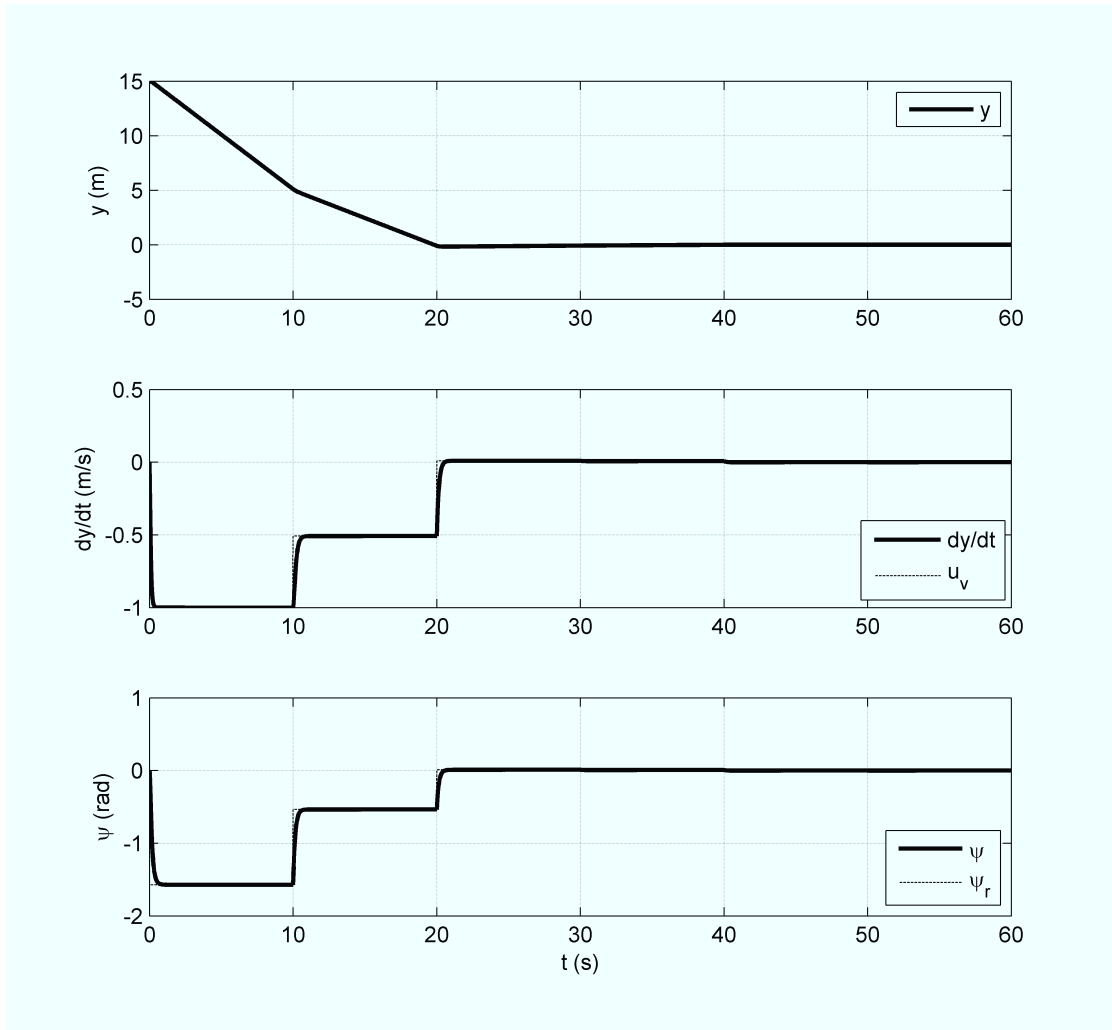
Figure 4.5: Unicycle dynamics simulation results

to u_v, that was assumed to be zero in Chapter 3.

4.2.5 Experimental results

Two experiments were performed using the HYCONS Rover. Table 4.4 summarizes the parameters that are common to both experiments. It is worth noting that the experiments were performed using the vision tracking system that was described in Chapter 1. Therefore, the distance units used in this subsection are camera pixels. The velocities along the y axis, however, are normalized with respect to the forward speed v, mapping it in the
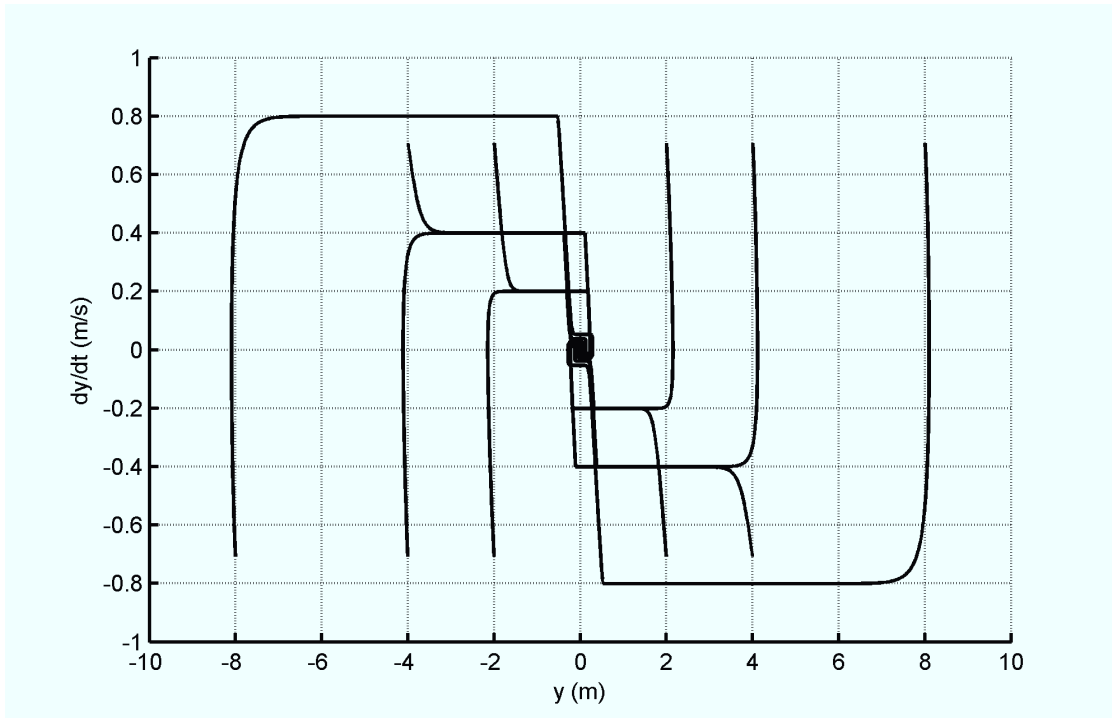
Figure 4.6: Phase plane plot of the unicycle's dynamics control

interval $[-1, 1]$.

Parameter	Value	Units
v	6.2	px/s
a	1	rad/s
k_ψ	5	—
τ_1	40	ms
τ_3	5	s

Table 4.4: HYCONS Rover experiment's parameters

In the first experiment, shown in Figure 4.7, the vehicle's initial position is $y = 220px$ and its heading is $\psi = 0.11rad$. After the command $u_p = 150$ is given at $t = 5s$, the commanded normalized velocity u_v is -1, which is its maximum value allowed by the saturation. This value provides a heading reference of $\psi_r = -\pi/2$. This reference is achieved in approximately $2s$. Subsequently, velocity and heading references are given every $5s$, when a new position is measured, making the vehicle's position converge to the reference in roughly $15s$ after the position reference is given. Although some noise from
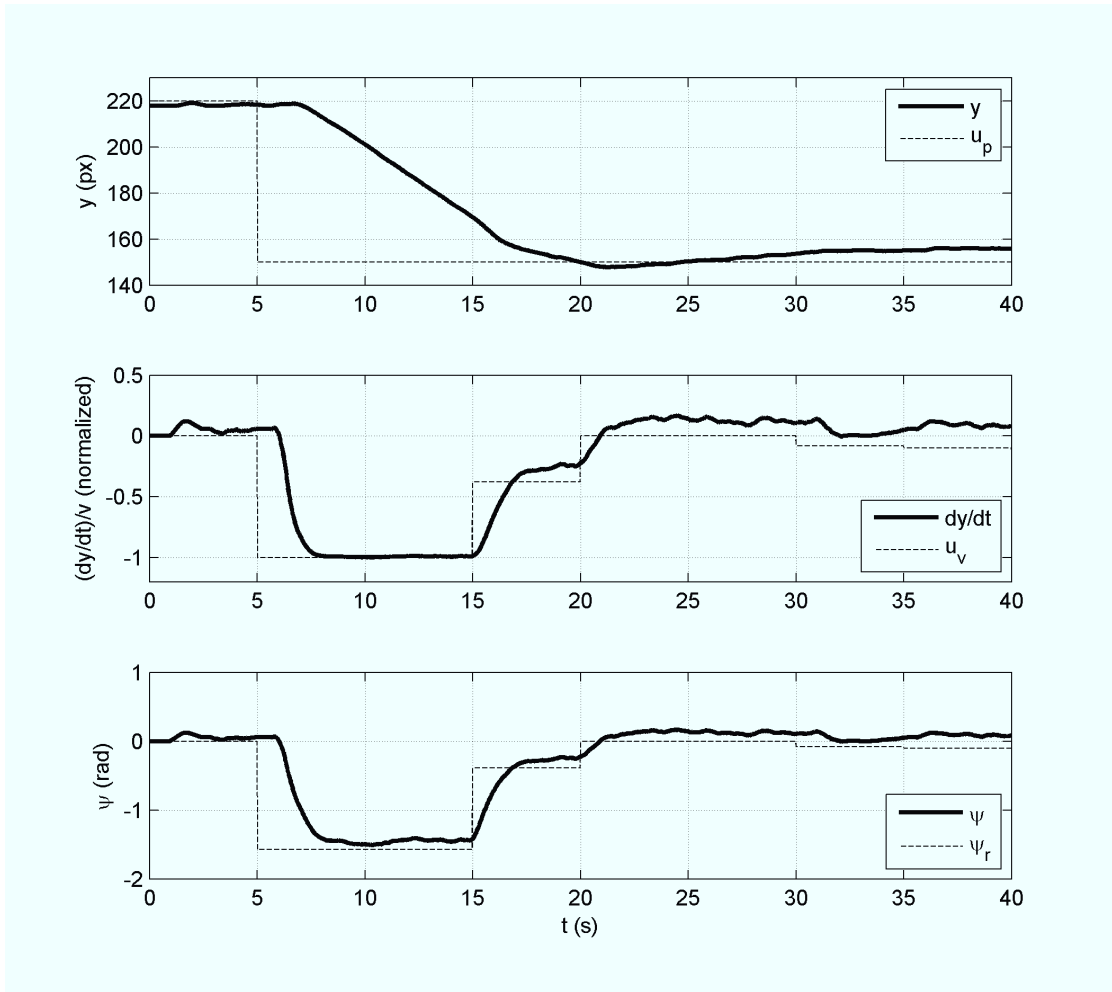
Figure 4.7: Experimental results obtained with the HYCONS Rover

the measurements is evident, the performance closely resembles the simulations, showing the robustness and practical relevance of the proposed multirate control technique.

The second experiment, shown in Figure 4.7 has different initial conditions. The vehicle's initial position is $y = 56px$ and its initial heading is $\psi = 0.06 rad$. The position reference is again $u_v = 150px$, which is reached roughly after $15s$, as in the first experiment.

For both experiments, it is possible to see that the system behaves very closely to what the simulations showed. Straight trajectories are clearly observed between sampling
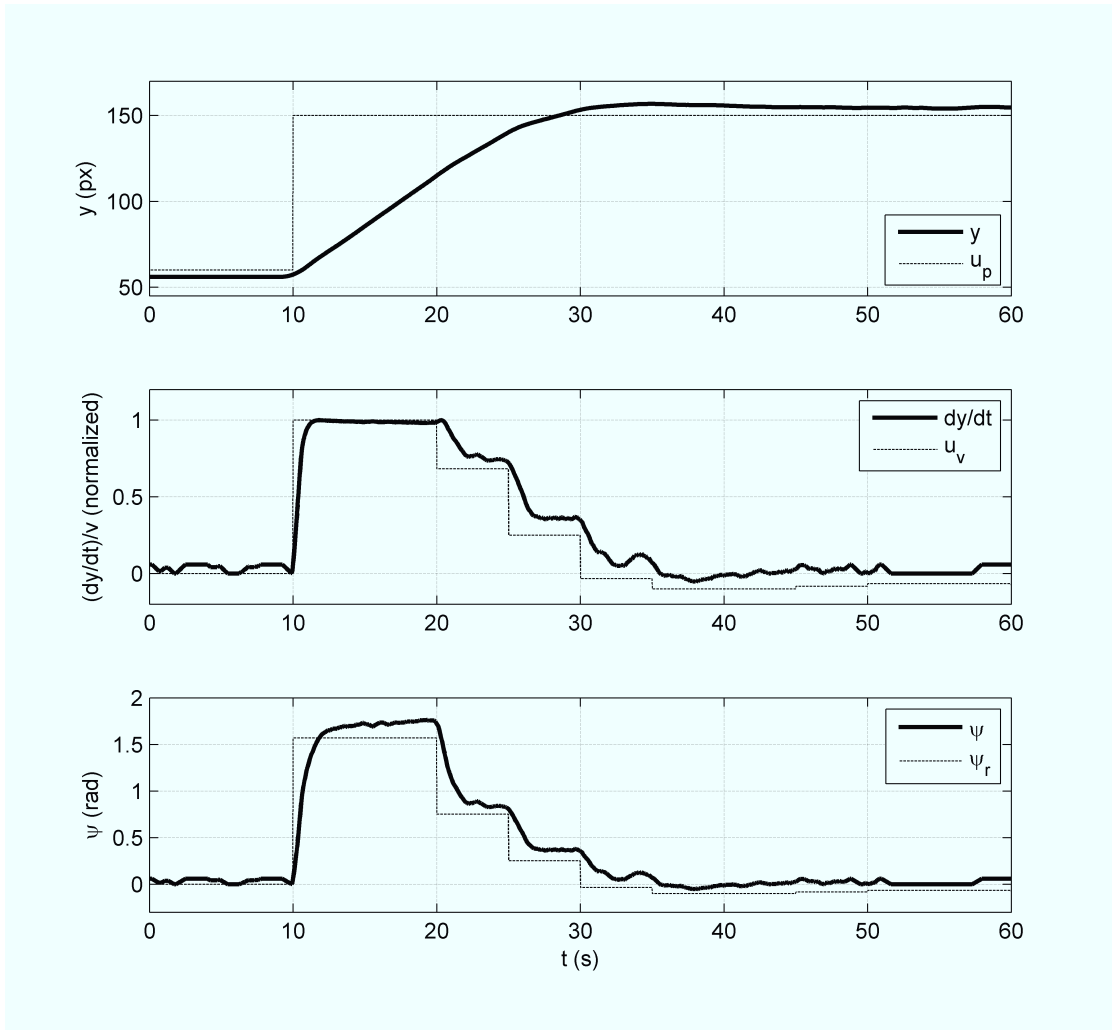
Figure 4.8: Further experimental results obtained with the HYCONS Rover

times, since constant velocities and heading references are given during such time intervals. The heading angle and velocity converges to the given references in a portion of the sampling period for position, τ_3. The implemented machine vision system has a rather low resolution compared to the HYCONS Rover's workspace; the resolution is of about $109px/m$, and therefore the feedback was affected by quantization error, and noise. The presented results were slightly filtered, using a moving average, to make the curves clear to the reader.

Next, a brief analysis of the Unicycle's control system is presented as a motivation to future work. It also provides an intuitive justification for Assumption U1.

4.2.6 Singular perturbations analysis

Singular perturbations analysis provides a theoretical foundation to the engineering practical approach of neglecting some terms of a system's model when they are considered to be small compared to the other magnitudes involved. In dynamical systems, this is relevant when multiple time scales are involved in a model, yielding "slow" and "fast" dynamics. The analysis presented in this subsection is based on [63].

Let us recall equation (3.21), which describes the dynamics of the unicycle model,

$$\begin{cases} \dot{y} = v sin(\psi) \\ \dot{\psi} = au \end{cases} \tag{4.32}$$

By using a continuous time linear controller to track a reference heading, we make

$$u = k_\psi(\psi_r - \psi) \tag{4.33}$$

and the system (3.21) becomes

$$\begin{cases} \dot{y} = v sin(\psi) \\ \dot{\psi} = ak_\psi(\psi_r - \psi) \end{cases}. \tag{4.34}$$

By letting

$$\varepsilon = \frac{1}{ak_\psi}, \tag{4.35}$$

we can rewrite system (4.34) as

$$\begin{cases} \dot{y} = v sin(\psi) \\ \varepsilon\dot{\psi} = \psi_r - \psi \end{cases} \tag{4.36}$$

As ak_ψ is made very large, then $\varepsilon \to 0$ and (4.36) can be analyzed as a singularly perturbed system. When $\varepsilon = 0$, neglecting the dynamics of the attitude control loop, the second line of equation (4.36) becomes the algebraic expression: $\psi = \psi_r$, and the system (4.36) reduces to

$$\dot{y} = v \sin(\psi_r) \tag{4.37}$$

which is exactly the Assumption U1, made in Chapter 3 and later removed in Chapter 4, where a heading-tracking controller was designed and this dynamics were considered in the analysis and simulations.

By comparing closely Figures 3.9 and 4.6, it is possible to see only very small differences in the trajectories of the states as a consequence of neglecting or considering the system's fast dynamics. Also, by carefully comparing Figures 3.8 and 4.5, it is possible to see small differences in the shapes of the curves, especially when a new position measurement is made, and new velocity and angle commands are computed. These two examples clearly show how the singularly perturbed system is an approximation of the original model.

Chapter 5

Conclusions

The main conclusions of this thesis are summarized in this final chapter, based on the contributions stated in Chapter 1. Potential future extensions of the work presented on this thesis are also proposed.

In Chapter 2, the conception, design and construction process was described, and a nonlinear model was presented. The vehicle was successfully designed and built, and its performance was satisfactory during both preliminary tests on ground and final flight tests. The attitude-tracking controller can stabilize the aircraft, allowing it to hover and navigate in indoor environments. Several different upgrades could be made to extend the capabilities of the HYCONS Quadrotor; however, the two following are proposed as the most immediate:

- Add a position-tracking sensor or system to the vehicle, and

- add environment ranging sensors.

With the addition of a position tracking system, the vehicle would be able to navigate completely autonomously in an environment, provided there are no obstacles in the commanded positions and possible trajectories. For indoor navigation, a tracking system based on infrared cameras is proposed. For outdoor navigation, a Global Positioning System (GPS) is proposed. On the other hand, environment ranging sensors would allow the

quadrotor to navigate in an environment even if there are obstacles in it, avoiding collisions and exploring different paths to complete a navigation control task.

In Chapter 3, the kinematics control of proposed multirate technique was discussed. It was shown in both analysis and simulation that the proposed approach successfully controls the two presented case studies under the assumption of directly controllable heading/attitude angles. For both case studies, the velocity along the axis of interest was shown to be controllable by modifying the heading/attitude angles. The velocity-controlled vehicle was shown to converge in a predictable number of steps to the commanded position under an arbitrarily low sampling frequency for the position loop. The following extensions are proposed as future work:

- Different paths that might take the vehicle faster to the commanded position can be explored, instead of using constant velocity commands that yield straight trajectories,

- Inter-sampling position estimation can be made based on the information from other states, the control inputs and a model.

The dynamics control was addressed in Chapter 4. The assumption of directly controllable heading/attitude angles was removed, and the analysis was carried out considering the rotational dynamics for both case studies. Angle-tracking controllers were designed to meet specific performance requirements that guarantee the overall stability of the proposed multirate system. The complete closed-loop system was derived and simulations for both case studies were performed, showing that the behavior of the angle-controlled system is very similar to the behavior of the systems under the assumptions made on Chapter 3. Experimental results were also presented, showing a performance that closely resembles the behavior that was expected from the simulations. The following extensions are proposed for future work:

- Formalize the conditions under which the dynamical system is guaranteed to be

69

stable without the assumptions made in Chapter 3 (Assumptions Q2 and U1).

- Extend the experimental results with a positioning system to perform fully autonomous navigation tests.

Bibliography

[1] J. N. Yelverton, "Wireless Avionics", *Digital Avionics Systems Conference*, 1995. 14th DASC. MA, USA, 1995.

[2] W. Kim, J. Biesiadecki, and K. Ali, "Visual Target Tracking on the Mars Exploration Rovers", International Symposium on Artificial Intelligence, Robotics and Automation in Space, CA, USA, 2008.

[3] P. Castillo, R. Lozano. A. Dzul, "Modelling and control of mini-flying machines". Springer, 2005.

[4] Adapted from the Wikimedia Commons file "Image:De Bothezat Quadrotor.jpg", URL:

[5] J. Boreinstein, "The HoverBot, An Electrically Powered Flying Robot" Unpublished White paper, University of Michigan, USA, 1992.

[6] I. Kroo, F. Prinz, et al, "The Mesicopter: A Miniature Rotorcraft Concept", Stanford University, USA, 2000.

[7] E. Altug, J.P. Ostrowski, R. Mahony, "Control of a quadrotor helicopter using visual feedback", Proceedings of the International Conference on Robotics and Automation, Washington DC, USA, 2002.

[8] A. Moktari, A. Benallegue, "Dynamic Feedback Controller of Euler Angles and Wind Parameters Estimation for a Quadrotor Unmanned Aerial Vehicle", Proceedings of the IEEE Conference on Robotics and Automation, 2004.

[9] A. Benallegue, A. Moktari, L. Friedman, "Feedback Linearization and High Order Sliding Mode Observer for a Quadrotor UAV", Proceedings of the International Workshop on on Variable Structure Systems, 2006.

[10] J. Dunfried, M. Tarbouchi, G. Labonte, "Neural Network Based Control of a Four Rotor Helicopter", Proceedings of the IEEE International Conference on Industrial Tecnhology, 2004.

[11] A. Tayebi, S. McGilvray, "Attitude Stabilization of a VTOL Quadrotor Aircraft", IEEE Transactions on Control Systems Technology, vol. 14, No. 3, May, 2006.

[12] K. Alexis, C. Papachristos, G. Nikolakopoulos, A. Tzes, "Model predictive quadrotor indoor position control", *19th Mediterranean Conference on Control and Automation*, Corfu, Greece, 2011.

[13] J. Wang, T. Bierling, L. Hocht, F. Holzapfel, "Novel Dynamic Inversion Architecture Design for Quadrocopter Control", *Advances in Aerospace Guidance, Navigation and Control*, Springer Berlin Heidelberg, 2011.

[14] L.R. Garcia-Carrillo, E. Rondon, A. Dzul, A. Sanche, R. Lozano, "Hovering quad-rotor control: A comparison of nonlinear controllers using visual feedback", *49th IEEE Conference on Decision and Control*, Atlanta, GA, USA, 2010.

[15] G.V. Raffo, M.G. Ortega, F.R. Rubio, "An integral predictive nonlinear H-infinity control structure for a quadrotor helicopter", *Automatica* 46, 2010.

[16] J. Toledo, L. Acosta, M. Sigut, J. Felipe, "Stabilisation and altitude tracking of a four-rotor microhelicopter using the lifting operators", *IET Control Theory and Applications*, Volume 3, issue 4, 2009.

[17] "ETH - IDSC - Flying Machine Arena." ETH. Web. 16 Apr. 2012. URL:

[18] D. Mellinger, N. Michael, V. Kumar, "Trajectory generation and control for precise aggressive maneuvers with quadrotors", International Journal of Robotics Research (Published online before print, doi: 10.1177/0278364911434236, January 25, 2012.

[19] H. Huang, G. Hoffmann, S. Waslander, C. Tomlin, "Aerodynamics and control of autonomous quadrotor helicopters in aggressive maneuvering", Proceedings of the IEEE International Conference on Robotics and Automation, ICRA '09, 2009.

[20] M. Muller, S. Lupashin, R. D'Andrea, "Quadrocopter Ball Juggling", IEEE/RSJ International Conference on Intelligent Robots and Systems, 2011.

[21] M. Hehn, R. D'Andrea, "Quadrocopter Trajectory Generation and Control", IFAC World Congress, 2011.

[22] S. Lupashin, R. D'Andrea, "Adaptive Open-Loop Aerobatic Maneuvers for Quadrocopters", IFAC World Congress, 2011.

72

[23] A. Schoellig, M. Hehn, S. Lupashin, R. D'Andrea, "Feasible Periodic Motion Primitives for Choreographed Quadrocopter Flight", American Control Conference (ACC), 2011.

[24] M. Hehn, R. D'Andrea, "A Flying Inverted Pendulum", IEEE International Conference on Robotics and Automation, 2011.

[25] P. Wiberg, U. Bilstrup, "Wireless technology in industry-applications and user scenarios", Proceedings of the 8th IEEE International Conference on Emerging Technologies and Factory Automation, 2001.

[26] R. Macedo, P. Carvalhal, J. Afonso, L. Silva, H. Almeida, M. Ferreiral, C. Santos, "A Fly-By-Wireless UAV Platform Based on a Flexible and Distributed System Architecture", IEEE International Conference on Industrial Technology, 2006.

[27] P. Carvalhal, M. Ferreira, L. Silva, H. Almeida, C. Santos, J. Afonso, "A Bluetooth-based Wireless Distributed Data Acquisition and Control System", IEEE International Conference on Robotics and Biomimetics, 2006.

[28] R. Yedavalli, R. Belapurkar, "Application of wireless sensor networks to aircraft control and health management systems", Journal of Control Theory and Applications, volume 9, issue 1, 2011.

[29] H. Liu, "Aircraft wireless sensor network for in-flight fault diagnostics and control", 3rd Annual IEEE/CANEUS Fly by wireless Workshop, Orono, ME, USA, 2010.

[30] N. Taajwar, S. Faruque, "Fly-By-CDMA wireless and single wire-line technology, a potential solution for Fly-By-Wireless/Less-wire", 4th Annual IEEE/CANEUS Fly by wireless Workshop, Montreal, Canada, 2011.

[31] T. Upal, S. Faruque, "Fly by wireless: An ultrasonic approach for UAV", 4th Annual IEEE/CANEUS Fly by wireless Workshop, Montreal, Canada, 2011.

[32] O. Elgezabal, C.Salazar, "Technological foundation for future intra-aircraft wireless applications: State of the art of wireless data transmission", 4th Annual IEEE/CANEUS Fly by wireless Workshop, Montreal, Canada, 2011.

[33] S. Chilakala, *Development and Flight Testing of a Wireless Avionics Network Based on the IEEE 802.11 Protocols*. MSc Thesis, University of Kansas, 2008.

[34] D. Hope, "Towards a Wireless Aircraft", PhD Thesis, University of York, UK, 2011.

73

[35] G. Kranc, "Input-output analysis of multirate feedback systems", IRE Transactions on Automatic Control, Volume 3, Issue 1, 1957.

[36] B. Friedland, "Sampled-data control systems containing periodically varying members", Proceedings of the 1st IFAC Congress, 1960.

[37] J. Johnson, C. Phillips, "Maximum errors from quantization in multirate digital control systems", AIAA Journal, American Institute of Aeronautics and Astronautics, Vol. 8, No. 4, 1970.

[38] D. Flowers, J. Hammond, "Simplification of the characteristic equation of multirate sampled data control systems", IEEE Transactions of Automatic Control, Vol. 17, Issue 2, 1972.

[39] W. Boykin, B. Frazier, "Multirate sampled-data systems analysis via vector operator", IEEE Transactions of Automatic Control, Vol. 20, Issue 4, 1975.

[40] D. Flowers, "Design techniques for a class of multirate sampled data control systems", Doctoral Thesis, Georgia Institute of Technology, 1972.

[41] A. Tangirala, D. Li, R. Patawardhan, S. Shah, T. Chen, "Ripple-free conditions for lifted multirate control systems", Automatica, Volume 37, Issue 10, 2001.

[42] H. Fijumoto, Y. Hori, A. Kawamura, "Perfect tracking control based on multirate feedforward control with generalized sampling periods", IEEE Transactions on Industrial Electronics, Volume 48, Issue 3, 2001.

[43] L. Yang, S. Yang, "Multirate Control in Internet-Based Control Systems", IEEE Transactions on Systems, Man, and Cybernetics, Part C: Applications and Reviews, Volume 37, Issue 2, 2007.

[44] H. Fujimoto, "Visual servoing of 6 DOF manipulator by multirate control with depth identification", Proceedings of the IEEE Conference on Decision and Control, 2003.

[45] S. Brittanti, F. Dell'Orto, A. Di Carlo, S. Savaresi, "Notch filtering and multirate control for radial tracking in high-speed DVD-players", IEEE Transactions on Consumer Electronics, Volume 48, Issue 1, 2002.

[46] Digi International Inc, "Digi XBee Wireless RF Modules".
URL: http://www.digi.com/xbee/

[47] DIY Drones, "XBee - Discussion forums - DIY Drones".
URL: http://diydrones.ning.com/forum/topic/listForTag?tag=xbee

[48] RC Groups, "Quadricopter with UDB4+GPS+XBee - RC Groups".
URL: http://www.rcgroups.com/forums/showthread.php?t=1590088

[49] Arduino Project Website, "Arduino Mega Board".
URL: http://arduino.cc/en/Main/ArduinoBoardMega

[50] MicroStrain Inc, "3DM-GX1 Product Datasheet".
URL: http://files.microstrain.com/3DM-GX1%20Datasheet%20Rev%201.pdf

[51] Castle Creations Inc, "Thunderbird Brushless Motors Controls".
URL: http://www.castlecreations.com/products/thunderbirds.html

[52] MaxBotix Inc, "MB1040 LV-MaxSonar-EZ4 Ultrasonic Rangefinder"
URL: http://www.maxbotix.com/products/MB1040.htm

[53] Simulink Block by Sergey Shapovalov, "RTsync Blockset - File Exchange - MATLAB Central"
URL: http://www.mathworks.com/matlabcentral/fileexchange/24975-rtsync-blockset

[54] Open Source Computer Vision - OpenCV Website. URL: http://opencv.willowgarage.com

[55] Horizon Hobby, "Park 370 Brushless Outrunner Motor, 1360Kv (EFLM1205): E-flite - Advancing Electric Flight".
URL: http://www.e-fliterc.com/Products/Default.aspx?ProdID=EFLM1205

[56] S. Bouabdallah, R. Siegwart, "Full Control of a Quadrotor", *Proceedings of the 2007 IEEE/RSJ International Conference on Intelligent Robots and Systems*, San Diego CA, USA, 2007

[57] K. Ogata, "Modern Control Engineering, 5th ed.", Prentice Hall, 2010.

[58] T. Bresciani, *Modelling, Identification and Control of a Quadrotor Helicopter*. MSc Thesis, Department of Automatic Control, Lund University, Sweden, 2008.

[59] M. Moarref, L. Rodrigues, "Asymptotic stability of piecewise affine systems with sampled-data piecewise linear controllers", Proceedings of the 50th IEEE Conference on Decision and Control, FL, USA, 2011.

[60] C. Ossa-Gómez, M. Moarref, L. Rodrigues, "Design, Construction and Fly-By-Wireless Control of an Autonomous Quadrotor Helicopter", *Proceedings of the 4th IEEE / CANEUS Fly-by-wireless Workshop*, Montreal, QC, Canada, 2011.

[61] C. Ossa-Gómez, L. Rodrigues, "Multi-Rate Sampled-Data Control of a Fly-by-wireless Autonomous Quadrotor Helicopter", *Proceedings of the 25th IEEE Canadian Conference on Electrical and Computer Engineering CCECE'2012*, Montreal, QC, Canada, 2012.

[62] L. Rodrigues, S., P., Boyd, "Piecewise-affine state feedback for piecewise-affine slab systems using convex optimization.", *Systems & Control Letters*, 54(9), 835–853, 2005.

[63] H. Khalil, *Nonlinear Systems, 3rd ed.* Prentice Hall, NJ, USA, 2002